The final publication is available at

https://doi.org/10.1016/j.jconrel.2020.04.045

Additional Information

Small

Preclinical antitumor efficacy of combined senescence-inducing chemotherapywith targeted nanotherapeutic senolysis
--Manuscript Draft--

Manuscript Number:	
Full Title:	Preclinical antitumor efficacy of combined senescence-inducing chemotherapywith targeted nanotherapeutic senolysis
Article Type:	Full Paper
Section/Category:	
Keywords:	
Corresponding Author:	Mar Orzaez Calatayud, PhD Centro de Investigación Príncipe Felipe Valencia, SPAIN
Additional Information:	
Question	**Response**
Please submit a plain text version of your cover letter here.	Dear Editor, We would like to submit our manuscript entitled "Preclinical antitumor efficacy of combined senescence-inducing chemotherapy with targeted nanotherapeutic senolysis" by Irene Galiana, María Alfonso, Andrea Bernardos, Beatriz Lozano-Torres, Mónica Sancho, Viviana Bisbal, Manuel Serrano, Ramón Martínez-Máñez,* Mar Orzáez* to Small. Senescence is a physiological process that causes a permanent cell cycle arrest (Hayflick L, Exp. Cell Res,1961). Different physiological processes or stimuli lead the cell to the entrance into this state (Lozano B, et al. Nat Rev Chem, 2019). In this context, senescence chemical inducers, such as Palbociclib, have recently reached clinics for the treatment of tumors in combination with conventional therapies (Sutherland RL, et al. Breast Cancer Res. ,2009; Finn RS, et al. Breast Cancer Res., 2009). However, recent research has revealed the negative consequences that the persistence of senescent cells in the body has on the development of tumors and the appearance of metastases (Wieland E, et al. Cancer Cell, 2017; Milanovic M, et al. Nature 2017; Parrinello S, et al. J. Cell Sci. 2005). Therefore, the design of new treatment strategies requires efficient elimination of remaining senescent cells (senolysis) upon therapeutic senoinduction (Kirkland JL, et al. J. Am. Geriatr., 2017; Zhu Y, et al. Aging Cell, 2016). Here, we report a combination of senogenesis (senoinduction with palbociclib) with nanoformulated targeted senolysis (encapsulated navitoclax) in triple negative orthotopic breast cancer mice model. Our results show that treatment of TNBC with palbociclib and further elimination of senescent cells with encapsulated navitoclax in galacto-oligosaccharide capped MSNs has benefit in tumour development, reduces metastases formation and has the additional benefit of diminishing navitoclax negative

	systemic toxicity that impedes its clinical translation. This aggressive mice model nearly recapitulates all the characteristics of the human TNBC, making the results obtained from this study particularly relevant in terms of clinical translation. We believe that our findings will attract a broad readership and could lead to the therapeutic targeting of senescent cells for improving chemotherapy outcome in breast cancer treatment. We hope that you will consider this manuscript for publication. Sincerely Yours, Mar Orzáez, PhD Ramón Martínez-Máñez, PhD
Do you or any of your co-authors have a conflict of interest to declare?	Yes
Please state: as follow-up to "Do you or any of your co-authors have a conflict of interest to declare?"	R.M. and M.S: are co-founder and shareholder of Senolytic Therapeutics, Inc. (USA) and Senolytic Therapeutics, S.L. (Spain).
Corresponding Author Secondary Information:	
Corresponding Author's Institution:	Centro de Investigación Príncipe Felipe
Corresponding Author's Secondary Institution:	
First Author:	Irene Galiana
First Author Secondary Information:	
Order of Authors:	Irene Galiana
	Maria Alfonso
	Andrea Bernardos
	Beatriz Lozano-Torres
	Monica Sancho
	Viviana Bisbal
	Manuel Serrano
	Ramón MArtínez-Mañez
	Mar Orzaez Calatayud, PhD
Order of Authors Secondary Information:	
Abstract:	Senescence induction produces a stable cell cycle arrest of cancer cells, arresting tumor growth and promoting immune clearance. However, incomplete clearance of senescent cells may favour tumor dormancy and recurrence, plausibly limiting the positive effects of these drugs in the long term. An approach to overcome this situation is the combination of senescence induction with the subsequent elimination of senescent cells. In this work, the antitumor efficacy of a combination therapy involving senogenesis and targeted senolysis, in an orthotopic immunocompetent model of the highly aggressive 4T1 triple negative breast cancer, has been explored. Senogenesis is induced with palbociclib, whereas senolysis is achieved with nano-encapsulated navitoclax. Treatment with palbociclib and further elimination of senescent cells with encapsulated navitoclax has demonstrated to delay or even prevent tumor growth, reduces metastases and has the additional benefit of diminishing the systemic toxicity of navitoclax. Conceivably, this principle could be applied to other senescence-

	inducing chemotherapies and tumor types.

WILEY-VCH

Preclinical antitumor efficacy of combined senescence-inducing chemotherapywith targeted nanotherapeutic senolysis

*Irene Galiana,[1,2] María Alfonso,[1] Andrea Bernardos,[1,2] Beatriz Lozano-Torres,[1,3] Mónica Sancho,[2,4] Viviana Bisbal,[4] Manuel Serrano,[6] Ramón Martínez-Máñez,[*1,2,3,5] Mar Orzáez[*2,4]*

e-mail: rmaez@qim.upv.es; morzaez@cipf.es

[1] Instituto Interuniversitario de Investigación de Reconocimiento Molecular y Desarrollo Tecnológico (IDM), Universitat Politècnica de València, Universitat de València. *Camino de Vera, s/n. 46022, Valencia, Spain.*
[2] Unidad Mixta UPV-CIPF de Investigación en Mecanismos de Enfermedades y Nanomedicina, Universitat Politècnica de València, Centro de Investigación Príncipe Felipe. *C/ Eduardo Primo Yúfera 3. 46012, Valencia, Spain.*
[3] CIBER de Bioingeniería, Biomateriales y Nanomedicina (CIBER-BBN).
[4] Centro de Investigación Príncipe Felipe. *C/ Eduardo Primo Yúfera 3. 46012, Valencia, Spain.*
[5] Unidad Mixta de Investigación en Nanomedicina y Sensores. Universitat Politècnica de València, IIS La Fe. *Av. Fernando Abril Martorell, 106 Torre A 7ª planta. 46026, Valencia, Spain.*
[6] Institute for Research in Biomedicine (IRB Barcelona), Barcelona Institute of Science and Technology (BIST), Catalan Institution for Research and Advanced Studies (ICREA), Barcelona, *Spain.*

Abstract: Senescence induction produces a stable cell cycle arrest of cancer cells, arresting tumor growth and promoting immune clearance. However, incomplete clearance of senescent cells may favour tumor dormancy and recurrence, plausibly limiting the positive effects of these drugs in the long term. An approach to overcome this situation is the combination of senescence induction with the subsequent elimination of senescent cells. In this work, the antitumor efficacy of a combination therapy involving senogenesis and targeted senolysis, in an orthotopic immunocompetent model of the highly aggressive 4T1 triple negative breast cancer, has been

1

explored. Senogenesis is induced with palbociclib, whereas senolysis is achieved with nano-encapsulated navitoclax. Treatment with palbociclib and further elimination of senescent cells with encapsulated navitoclax has demonstrated to delay or even prevent tumor growth, reduces metastases and has the additional benefit of diminishing the systemic toxicity of navitoclax. Conceivably, this principle could be applied to other senescence-inducing chemotherapies and tumor types.

1. Introduction

Cellular senescence can be defined as a state of stable cell cycle arrest in response to stressful stimuli.[1,2] As senescent cells become cell-cycle arrested, senescence has appeared as a desirable outcome in tumor treatment. Thus, several senescence-inducing or senescence-reinforcement drugs have been developed, including telomerase activity inhibitors, tumor suppressor gene re-activators or cyclin dependent kinase (CDKs) inhibitors.[3,4] In fact, CDK4/6 inhibitors abemaciclib,[5] palbociclib [6] and ribociclib [7] have been recently approved by the Food and Drug Administration (FDA) for the treatment of estrogen receptor (ER)-positive metastatic breast cancer in combination with anti-hormonal therapy, showing the best progression-free survival (PFS) results obtained to date.[8–10] Specifically, palbociclib is an oral highly specific inhibitor that blocks CDK4- and CDK6- cyclin D kinase activity at very low concentrations.[6,11] Moreover, given the pre-clinical results obtained [6] and after several clinical trials,[9,12–17] palbociclib is currently prescribed as a combination therapy with either letrozole or fulvestrant for the treatment of ER+/Her2- advanced breast cancer patients and is in clinical trials for the treatment of triple negative breast cancer (TNBC) patients overexpressing the androgen receptor (AR). TNBC patients are a subgroup of particular interest as TNBC is considered one of the

most aggressive and with poorer prognosis of the breast cancer subtypes with few treatment options.

Despite the clinical potential of senescence inducers, it is now well-established that the role of senescent cells can be either beneficial or detrimental regarding their implication in age-related diseases or cancer,[18] phenomenon known as antagonistic pleiotropy.[19] When cell damage takes place, during cancer or aging, senescent cells initiate a sequence of processes involving the immune system that culminates in senescent cells clearance and tissue regeneration. Nevertheless, this beneficial process can be corrupted, particularly in aged tissues when the immune system may become impaired. When senescent cells cannot be efficiently eliminated, their accumulation aggravates tissue dysfunction, causes ineffective tissue regeneration and contributes to several diseases.[20–24] The antagonistic pleiotropy character of senescence is also reflected in the role of the secretory associated senescence phenotype (SASP) as it is thought to participate in the clearance of pre-malignant cells, reinforcing the senescence state and participating in tissue remodelling and repair; but it can also contribute to tumor progression by stimulating phenotypes associated with aggressive cancer cells, providing an ideal niche for cancer cells proliferation or contributing to the epithelial-to-mesenchymal transition.[1,21,23] Senescence can therefore be a double-edged sword by either suppressing or promoting tumor development.[24–27] For all these reasons, if senescent cells remain in the organism and accumulate, they can become a potential risk for future carcinogenesis and metastasis.[28–30] Therefore, in relation to cancer, the long-term improvement of chemotherapy and senescence-inducing treatments inevitably involves the elimination of senescent cells.[31]

There are two main therapeutic approaches to attenuate senescence negative effects: senolysis induction, that provokes the direct elimination of senescent cells; and SASP neutralization.[24,32]

Regarding senolysis, a selective and universal method for the elimination of senescent cells would be a potentially useful therapy, but no such senolytic drugs are yet approved. Nevertheless, a number of small molecules are known to have senolytic effect both *in vitro* and *in vivo* models.[33] Among them, navitoclax is a potent specific inhibitor of the anti-apoptotic proteins Bcl-2, Bcl-w and Bcl-xL.[34] The survival of senescent cells is highly dependent on the elevated levels of the BCL-2 family of anti-apoptotic factors, and this makes them hypersensitive to apoptosis induced by Bcl-2 inhibitors.[34–37] Of note, the Bcl2 family inhibitor navitoclax, one of the most potent senolytic drugs, has some toxic side effects that prevent the FDA from approving its clinical use. In particular, its major dose-limiting toxicity is thrombocytopenia, an effect derived from the inhibition of Bcl-xL.[38,39]

From another point of view, the design of nanomaterials as drug carriers with improved pharmacokinetics, bioavailability and biodistribution has revolutionized the field of controlled drug delivery systems in the last years. Among different nanocarriers, mesoporous silica nanoparticles (MSNs) have proven to be excellent scaffolds to develop multifunctional nanodevices for advanced medical applications, thanks to their advantageous characteristics such as homogeneous porosity, inertness, high loading capacity and easy surface functionalization. Moreover, MSNs can be gated with different molecular ensembles resulting in nanodevices showing "zero" release that can be opened on-command upon the application of specific physical, chemical or biochemical stimuli.[40–42] MSNs have been specially used for cancer treatment as they can passively accumulate in tumors due to the enhanced permeability and retention (EPR) effect. Moreover and due to their cargo release triggering ability, they can direct the protected cargo to specific targeted sites, thus reducing associated side effects in healthy tissues.[43–45] In previous collaborative works of our group, capped MSNs have already been

4

tested in several senescence-related diseases models such as dyskeratosis congenital,[46,47] chemotherapy-treated xenograft tumors or lung fibrosis.[48]

We report herein a combination of senogenesis with targeted senolysis in an orthotopic and immunocompetent triple negative breast cancer model. Senogenesis is induced with the CDK4/6 inhibitor palbociclib, and senolysis is achieved with navitoclax encapsulated in MSNs capped with a galacto-oligosaccharide. Similar nanoparticles loaded with the dye indocyanine green are also used to trace senescence *in vivo*. We show that treatment of TNBC with palbociclib and further elimination of senescent cells with encapsulated navitoclax has benefit in tumor development, reduces metastases formation and has the additional added benefit of diminishing navitoclax negative systemic toxicity.

2. Results

2.1. Palbociclib induces senescence in 4T1 triple negative breast cancer cells

The 4T1 murine breast cancer cell line has a triple negative highly aggressive profile and the in vivo model recapitulates many aspects of the human disease.[49–52] The relevance of immunity in the antitumoral response, and particularly upon senescence induction, makes fundamental performing studies of tumor evolution in the presence of an intact immune system.[53,54] For this reason, we considered the use of this orthotopic immunocompentent breast cancer murine model to develop in vivo studies of senoinduction and senolysis.

Only some subtypes of triple negative breast tumors respond properly to treatment with CDK4/6 inhibitors.[55] Thus, we first determined the sensitivity of 4T1 TNBC cell line to treatment with palbociclib. We found that treatment with 5μM palbociclib produced the appearance of canonical senescence markers in the 4T1 cells, such as the overexpression of the lysosomal β-galactosidase

enzyme (SA-βGal) [56,57] (**Figure 1A**) that was accompanied by an increase in cell size and higher number of intracellular vesicles, in agreement to morphological features described for senescent phenotype.[1,20,32] Reduced immunostaining of the Ki67 proliferation marker, indicative of cell cycle arrest, was also detected (**Figure 1B**) together with a progressive decrease in the phosphorylation of the retinoblastoma protein (pRb) (**Figure 1C**). To further confirm cycle arrest in 4T1 palbociclib-treated cell cultures, clonogenic assays were also performed. To this end, the same number of control and senescent cells were initially seeded in culture plates and, one week later, the increase of cell number was estimated by crystal violet staining. 4T1 cell cultures treated with palbociclib showed less staining, indicative of decreased cellular proliferation and consistent with cellular arrest (**Figure 1D**). All together, these results confirmed that senescence was efficiently induced by the CDK4/6 inhibitor palbociclib in the 4T1 triple negative murine breast cancer cell line.

2.2. Senolysis in 4T1 breast cancer senescent cells

Senescent cells are highly dependent on various pro-survival factors. In particular, the dependence on the anti-apoptotic protein Bcl-xL has been reported in different cell lines.[58] We wondered if overexpression of this anti-apototic Bcl-2 family protein member was also taking place in 4T1-palbociclib treated cells. To address this question we analysed changes in protein expression of Bcl-xL as a consequence of palbociclib treatment. The levels of the anti-apoptotic member increased significantly as a consequence of senescence induction (**Figure 2A**). This increase was accompanied by an increment in the expression of pro-apoptotic BH3-only protein Bim. The obtained Bcl-2 protein profile was consistent with a phenotype attributed to "primed

cells", which show a high dependence on anti-apoptotic proteins for survival and become highly sensitive to BH3 mimetics drugs such as navitoclax.[59,60]

Inhibition of Bcl-2 anti-apoptotic proteins by free navitoclax (Nav) was then explored as a strategy to selectively induce cell death in 4T1-senecent cells. First, mitochondrial functionality upon treatment of 4T1 cells with free navitoclax was analysed by flow cell cytometry using the membrane-permeable dye JC-1.[61] JC-1 dye accumulates in the mitochondria in a potential dependent manner, shifting the fluorescence emission maximum from green to red. A decrease in the population of cells with a high red/green fluorescence ratio is indicative of a loss of mitochondrial functionality. Palbociclib-induced 4T1 senescent and control cells were treated with navitoclax and mitochondrial membrane potential changes were analyzed. Senescent cells showed a reduced mitochondrial membrane potential when compared with non-treated cells (**Figure 2B**), which is in agreement with other reported studies with senescent cells.[62–64] Upon treatment with navitoclax, a further decrease in mitochondrial potential was observed (Figure 2B) and it was accompanied by a selective cell death induction (**Figure 2C**) only in the 4T1-senescent cultures. In fact, the IC50 of navitoclax was 0.3µM for senescent cultures, while this drug concentration did not produce cell death in normal cultures that presented a considerable higher IC50 concentration. Senolytic activity at the IC50 was also confirmed either by crystal violet cell cytotoxicity assays (**Figure 2D**) and by flow cytometry, quantifying dead cells that exposed phosphatidyl-serine to the outer plasma membrane leaflet in an Annexin V FITC binding assay (**Figure 2E**). Both studies confirmed the selectivity of navitoclax for inducing cell death in senescent cells. Finally, a caspase 3/7 activity detection assay confirmed that the cell death that occurred after navitoclax treatment was triggered via apoptosis (**Figure 2F**).

On the basis of the mesoporous silica nanoparticles advantages, navitoclax was encapsulated in MSNs capped with a hexa-galacto-oligosaccharide molecule obtaining the loaded nanoparticles **Gal·NP(Nav)** (**Figure 3A**). Considering that senescent cells are characterized by high levels of lysosomal β-galactosidase activity (SA-βGal), the galacto-oligosaccharide acts as a "molecular gate" that is expected to be hydrolysed in senescent cells by the action of this senescence-associated β-galactosidase activity. Similar capped nanoparticles were loaded with the fluorescent dye indocyanine green (ICG), referred to as **Gal·NP(ICG)**.

TEM images of the nanoparticles showed spherical particles of ca. 80-100nm in which the channels of the MCM-41 matrix were visualized as alternate black and white stripes or as a honeycomb porous structure (**Figure 3B**, **Figure S3**). N_2 adsorption-desorption studies confirmed the presence of uniform cylindrical mesoporous in the starting MSNs, with a pore size of 2.8 nm and a total specific surface of 1091 m^2 g^{-1} (**Table S1**). Moreover, a significant decrease in the adsorbed N_2 volume and surface area was observed in the loaded **Gal·NP(ICG)** nanoparticles (57 m^2 g^{-1}) which confirmed cargo loading inside the pores (**Figure S4**). From dynamic light scattering (DLS) measurements (**Figure S5**), the hydrodynamic diameter of the starting MSNs and the final **Gal·NP(ICG)** were determined to be 183 nm and 376 nm, respectively (**Table S2**), with a single population distribution which indicated the good dispersion of the particles. This increase in the hydrodynamic diameter, as well as the increase in zeta potential values, was consistent with the external functionalization of the nanoparticles with the galacto-oligosaccharide, and also occurred in **Gal·NP(Nav)** (301 nm) and in the capped nanoparticles without cargo **Gal·NP(0)** (249 nm). Moreover, experiments with both **Gal·NP(ICG)** and **Gal·NP(Nav)** demonstrated efficient cargo capping and a selective and effective release in the presence of fungal β-galactosidase due to enzymatic hydrolysis of the

8

capping galacto-oligosaccharide (**Figure S6** and **Figure 3C**, respectively). For **Gal·NP(Nav)** nanoparticles, termogravimetrical and HPLC studies indicated that there were 141.4mg of galactoologisaccharide per gram of solid, and that 60 mg of navitoclax were delivered per gram of nanoparticles in the presence of β-galactosidase.

Gal·NP(ICG) nanoparticles were validated in the 4T1 murine breast cancer cell line by confocal microscopy and flow cytometry. Both studies showed that **Gal·NP(ICG)** released their content more efficiently in palbociclib-senescent cells compared to control cells after 6 or 24 hours (**Figure 3D**, **Figure S7**), in concordance with their high levels of β-galactosidase activity. The ICG probe is located in a perinuclear region consistent with the release of the drug in the lysosomal compartment. In a next step, the navitoclax-loaded nanoparticles **Gal·NP(Nav)** were also tested in 4T1 cells. Treatment of control and senescent 4T1 cells with increasing concentrations of the nano-senolytic **Gal·NP(Nav)** caused a selective decrease in senescent cells viability with an IC50 of 0.07μM of navitoclax, which is significantly lower than that obtained for the free drug (0.3μM) (**Figure 3E**). Crystal violet staining of cells treated with **Gal·NP(Nav)** at the free navitoclax IC50 concentration confirmed the selective induction of cell death in senescent cells (**Figure 3F**). Finally biocompatibility studies with capped nanoparticles with no cargo, **Gal·NP(0)**, showed that empty nanoparticles were harmless for 4T1 cells at 72h for all studied concentrations (**Figure S8**). Hence, oligosaccharide-capped nanoparticles demonstrated suitable to deliver ICG preferentially in palbocliclib-induced 4T1 senescent cells and navitoclax enhanced its senolytic activity when encapsulated, demonstrating the functionality of the encapsulation method.

2.3. *In vivo* imaging and treatment of 4T1 triple negative breast cancer tumors

Once demonstrated the capability of palbociclib to induce senescence in the 4T1 cellular model, we moved one step forward to study the combination of senogenesis (senoinduction by palbociclib) with targeted senolysis (using **Gal·NP(Nav)** and free navitoclax) in a triple negative orthotopic breast cancer model, aiming to improve antitumor efficacy. Studies with the dye-loaded **Gal·NP(ICG)** nanoparticles were also carried out.

Balb/cByJ female mice (4-6 weeks) were injected in the mammary pads with 4T1 cells for tumor formation. After one week of free tumor growth, palbociclib treatment started by daily oral gavage for one week (50mg/kg) (**Figure 4A**). Senescence induction was efficiently achieved in palbociclib treated animals, as inferred from the increase in SA-βGal activity that was observed in the tumors (**Figure 4B**). Senescence was also confirmed immunohistochemically in tumor sections, where the expression of the proliferative marker Ki67 decreased in palbociclib treated tumors as a consequence of cell cycle arrest associated to the senescent status (**Figure 4C**).

To validate the preferential in vivo cargo delivery by the capped nanocarriers, animals were intraperitoneally administrated with **Gal·NP(ICG)** after 1 week of palbo treatment. In vivo imaging studies of the probe distribution 24h post-injection clearly showed the preferential accumulation of the fluorescent dye in palbociclib-treated tumors (**Figure 4D**), with only a mild signal over the background observed in tumors non-treated with palbociclib but administrated with **Gal·NP(ICG)**. Moreover, the biodistribution of the nanoparticles was studied by the determination of silicon in different organs by inductively coupled plasma mass spectroscopy (ICP-MS) (**Figure 4E**). Interestingly, the levels of silicon indicate that nanoparticles accumulate both in senescent and non-senescent tumors. Enhanced dye signal in palbociclib-treated tumors is therefore consequence of β-galactosidase-induced dye delivery from **Gal·NP(ICG)** (note that

the dye is strongly auto-quenched inside the capped nanoparticles).[43–45] Overall this demonstrated that **Gal·NP(ICG)** can be of use for the detection of senescence by optical *in vivo* imaging.

After demonstrating that oligosaccharide capped nanoparticles preferentially release the fluorescent dye ICG in senescent tumors, we wondered whether encapsulated senolytic navitoclax would also target senescent cells in vivo in the TNBC model. Three days after 4T1 cells orthotopic injection, mice were treated with palbociclib when a visible tumor was evident on the mammary pads of the animals. One day after initiating palbociclib administration, either free navitoclax or encapsulated **Gal·NP(Nav)** was administered for 16 days (**Figure 5A**). Treatment efficacy and safety was monitored by measuring tumor size and body weight every two days.

All groups receiving palbociclib treatment significantly reduced tumor size in comparison with non-palbociclib treated groups (**Figure 5B**). In fact, groups that were not treated with the CDK4/6 inhibitor (Control, Nav or **Gal·NP(Nav)**) reached the humane endpoint at day 15 of palbociclib treatment (**Figure 5D**). It is important to note that the senolytic treatments had no effect on the tumors in the absence of senogenic treatment with palbociclib. Tumor size reduction by palbociclib is of particular interest, as on-going clinical trials with palbociclib in combination with bicalutamide in triple negative breast cancer patients are focused on patients overexpressing the androgen receptor (AR) (Clinical Trial ID: NCT02605486).[55] Noticeably, the 4T1 cell line does not express the AR receptor (**Figure S10**), so the observed palbociclib antitumoral activity in vivo in the 4T1 TNBC model suggest the potential application of this drug to novel subgroups of TNBC patients, and evidences the necessity to look for new biomarkers of drug sensitivity.

Concerning co-treatments with the senescence inductor palbociclib plus the senolytic navitoclax, interestingly **Gal·NP(Nav)** had a therapeutic benefit in combination with palbociclib, whereas treatment with only **Gal·NP(Nav)** displayed no effect, demonstrating that the therapeutic effect of **Gal·NP(Nav)** requires the induction of senescence (Figure 5B and **5C**). Animals treated with palbociclib and free navitoclax died or reached human end point at day 15.

Activation of cell death was assessed by immunofluorescence assays of active caspase 3 in tumor sections (**Figure 5F**) demonstrating that apoptosis was occurring in **Gal·NP(Nav)** co-treated tumors due to navitoclax release. In addition, all palbociclib plus **Gal·NP(Nav)** treated animals survived until the end of the experiment without relevant changes in body weight (**Figure S9**). In contrast the combination of palbociclib and free navitoclax produced a clear decrease in animal survival (**Figure 5D**) and those animals that survived had to be euthanatized before the end point of the study due to an excessive weight loss (more than 10%). This is indicative of a reduction in navitoclax toxicity when encapsulated. Another important result to highlight was that **Gal·NP(Nav)** co-treated animals presented a reduction in the number of lung metastases when compared to mice only treated with palbociclib (**Figure 5E**). This is remarkable as metastases formation is one of the most common consequences in human breast cancer. Collectively, we conclude that encapsulation of the senolytic drug navitoclax produces a benefit in tumor development and metastases formation, with the added benefit of reducing drug negative side-effects.

3. Discussion and conclusion

Senescence has been traditionally considered an evolutionary strategy to avoid tumor proliferation. Based on this vision, antitumoral senescence inducing agents have evolved and

reached clinics. However, as knowledge has advanced the double-edged sword role of senescence in cancer evolution has been evidenced. Recent reports have shown that traditional chemotherapeutics, such as doxorubicin and radiotherapy, cause senescence in tumors.[3] This therapy induced senescence could have both positive and negative consequences for patients. On one hand, senescent cells are eliminated by macrophages, and contribute to the generation of anti-tumoral immune responses; while on the other hand they are a source of inflammatory signalling molecules that shape the microenvironment towards pro-carcinogenesis, supporting tumor cell spreading. In terms of benefits, a seminal study showed that genetic clearance of p16INK4A - expressing senescent cells increases survival of mice with tumors at the time of death.[65] Since then, it has been demonstrated that a number of diseases are associated with the presence of senescent cells and that their elimination is beneficial in mouse models. However, it has not been properly addressed how the dual behaviour of senescence could be affecting those treatments that actively produce senescence in tumors and that are currently in clinical use, such as the CDK4/6 inhibitor palbociclib. Considering these circumstances there is a clear potential for treatment improvement that needs to be addressed. In this work we demonstrate that a combination of senogenesis (senoinduction with palbociclib) with nanoformulated targeted senolysis (encapsulated nanvitoclax) in triple negative orthotopic breast cancer mice model improves antitumor efficacy, metastases reduction and reduce navitoclax negative toxicity. This aggressive mice model nearly recapitulates all the characteristics of the human TNBC, making the results obtained from this study particularly relevant in terms of clinical translation.

The encapsulated nanodevice consists of spherical mesoporous silica nanoparticles of ca. 100 nm diameter, loaded with navitoclax and capped with galacto-oligosaccharides that prevent cargo delivery from the porous silica matrix (**Gal·NP(Nav)**). Similar galacto-oligosaccharides-capped

13

nanoparticles have proved suitable for selectively deliver certain cargos in senescent cells. Selective opening and delivery is based on the high levels of lysosomal β-galactosidase activity present in senescent cells in diseased and damaged tissues. β-galactosidase hydrolysis of the cap induces pore opening and payload release. On the basis of the mesoporous silica nanoparticles advantages, we also prepared capped nanoparticles loaded with the fluorescent dye indocyanine green, **Gal·NP(ICG)**.

In terms of palbociclib treatment we demonstrate that senescence was efficiently induced by the CDK4/6 inhibitor palbociclib in the 4T1 triple-negative murine breast cancer cell line that do not express the androgen receptor. As stated above, on-going clinical trials with palbociclib in triple negative breast cancer patients are today focussed on patients overexpressing the AR, so our result suggests that there is still room for the potential application of palbociclib to novel subgroups of TNBC patients. Cellular studies also demonstrate that **Gal·NP(ICG)** nanoparticles released their content more efficiently in palbociclib-senescent cells compared to control cells, in concordance with their high levels of β-galactosidase activity. Moreover, treatment of 4T1 cells with **Gal·NP(Nav)** induce a selective decrease in senescent cells viability which is significantly lower than that found for the free navitoclax. Moreover, capped nanoparticles with no cargo are harmless for 4T1 cells at 72h.

In vivo imaging studies of the **Gal·NP(ICG)** distribution 24h post-injection clearly show the preferential accumulation of fluorescent dye in palbociclib-treated tumors, which is corroborated by the determination of silicon in different organs by inductively coupled plasma mass spectroscopy. This demonstrates our nanoparticles can be of use for the detection of senescence by *in vivo* imaging.

Moreover, the nanoparticles loaded with navitoclax (i.e **Gal·NP(Nav)**) have a therapeutic benefit in combination with palbociclib. Encapsulation of navitoclax in the nanoparticles contributes to significantly reduce navitoclax toxicity. Animals treated with the combination palbociclib plus **Gal·NP(Nav)** survive to the in vivo experiment without relevant changes in body weight, whereas mice treated with palbociclib and free navitoclax showed a decrease in animal survival and weight loss. Besides, animals treated with palbociclib and **Gal·NP(Nav)** present a decreased number of lung metastases when compared to mice only treated with palbociclib, which is a remarkable result in terms of long survival prognosis.

Reduction of tumor size observed upon senolysis could be explained in different terms: i) the immune surveillance system is overloaded as consequence of continuous palbociclib induced senescence, and the senolytic drug contributes to help to senescent cells elimination; ii) chronically induced senescent cells actively evade the immune system and senolysis represents an alternative contribution to their elimination; iii) senolysis acts as an adjuvant therapy activating immune surveillance and favoring senescent cells elimination. However, the extent to which these mechanisms contribute to tumor reduction remains to be elucidated. Further studies addressing these questions would contribute to outline new antitumor strategies.

4. Experimental section

Chemicals and nanoparticles synthesis

Tetraethyl orthosilicate (98%), n-cetyltrimethylammonium bromide (CTAB) (≥99%), sodium hydroxide (NaOH) (≥98%), (3-aminopropyl)trimethoxysilane (APTES) (95%), anhydrous acetonitrile, anhydrous dichloromethane, indocyanine green (ICG), were purchased from Sigma-Aldrich. Galactan (from potato) was purchased from Carbosynth, and navitoclax was purchased from MedChemExpress.

Synthesis of the mesoporous silica nanoparticles (NPs scaffolds) was performed following reported procedures, as previously described by Muñoz-Espín *et al*,[48] with some modifications. For ICG-loaded nanoparticles, 0.4g of NPs scaffolds were added to a stirred solution of indocyanine green (ICG) (0.019g, 0.024 mmol) in 90mL of water. After 24h, the mixture was filtered and dried under vacuum. Nanoparticles were the functionalized by addition of APTES (0.4mL, 1.8 mmol) to a suspension of 0.3g of loaded scaffolds in 11mL of anhydrous MeCN. After 5.5h stirring at room temperature, the solid was isolated by filtration and dried under vacuum. For coating the scaffolds, 0.3g of functionalized nanoparticles were suspended in a solution of β(1,4)-galacto-hexasaccharide (0.74g, 1.4 mmol) and 40mL of water. After stirring for 21h at room temperature, the final product, referred to as **Gal·NP(ICG)** was filtered, washed with plenty of water and dried under vacuum. The same APTES functionalization and β(1,4)-galacto-hexasaccharide coating steps were performed to obtain the capped nanoparticles without load, referred to as **Gal·NP(0)**.

For navitoclax-loaded nanoparticles, 0.3g of NPs scaffolds were added to a solution of navitoclax (0.23g, 0.24 mmol) in 10mL of anhydrous dichloromethane, and the suspension was stirred at room temperature for 24h. Then, in the functionalization step, APTES (0.42mL, 1.8 mmol) was added to the suspension, and the stirring was kept for a further 5.5h. The obtained product was isolated by filtration under vacuum. For coating the functionalized navitoclax-loaded scaffolds, the same procedure as in the synthesis of **Gal·NP(ICG)** was followed. The final product referred to as **Gal·NP(Nav)** was isolated by filtration and washed with plenty of water and cold EtOH.

All the synthesized solids were stored in a desiccant at room temperature. A schematic representation of the described synthesis procedure is reflected in **Figure S1**.

Gal·NP characterization methods

Powder X-ray diffraction (PXRD), transmission electron microscopy (TEM), N_2 adsorption-desorption isotherms, thermogravimetric analysis (TGA), UV-visible and emission spectroscopy techniques were used were employed for materials characterization. PXRD measurements were performed on a Seifert 3000TT diffractometer using CuKα radiation at low angles ($1.3 < 2\theta < 8.3$, with steps of 0.04 degrees and 3 seconds for step) and high angles ($35 < 2\theta < 80$, with steps of 0.04 degrees and 1 second for step). Thermogravimetric analyses were carried out on a TGA/SDTA 851e Mettler Toledo equipment, using an oxidant atmosphere (air, 80 mL/min) with a heating program consisting on a heating rate of 10°C/min from 393K to 1273K and an isothermal heating step at this temperature for 30 min. For high resolution TEM imaging, samples were deposited on copper grids covered with carbon film provided by Electron Microscopy Sciences, and were recorded with 200 KV in a JEOL JEM-2100F microscope equipped with a X ray detector. N_2 adsorption-desorption isotherms were recorded on a Micromeritics TriStar II Plus automated analyser. Samples were previously degassed at 40°C in vacuum overnight and measurements were performed at 77K. The specific surface areas were calculated from the adsorption data in the low pressures range using the BET model. Pore size was determined by following the BJH method. Dynamic light scattering (DLS) measurements were carried out in a Malvern Zetasizer Nano ZS. UV-visible spectroscopy was carried out with a Lambda 35 UV/Vis spectrometer (Perkin-Elmer Instruments), and fluorescence spectroscopy was performed with a JASCO spectrofluorometer FP-8300.

Cargo release studies from Gal·NP(Nav)

4mg of **Gal·NP(Nav)** were suspended in 10mL of water at pH 4.5, stirred and this volume was separated into two suspensions of 5mL. Then, aliquots of 200µL were taken and 300µL of ethyl acetate were added to each one. The mixture was stirred for 1min, the ethyl acetate was taken, centrifuged and measured by UV-visible spectroscopy. Then, 5mg of β-galactosidase from *Aspergillus oryzae* were added to one of the aliquots, and, after certain time (1h, 3h, 5h...) 300µL of ethyl acetate was added to each one, stirred for 1 min, organic phase was taken, centrifuged and cargo released in organic phase was measured. Cargo release studies from **Gal·NP(ICG)** were also performed, and are resumed in **Figure S6**.

Cell lines

Cell line 4T1 (*mus musculus* mammary gland) was obtained from American Type Culture Collection (ATCC) and maintained in Dulbecco's modified Eagle's medium (DMEM, Sigma) supplemented with 10% fetal bovine serum (FBS), at 37ºC humidified atmosphere with 5% CO2. For senescence induction, medium was supplemented with palbociclib (#S1116, Selleckchem) at 5µM for 7 days.

β-galactosidase activity staining

Both 4T1 cultured cells and whole tissues (frozen tumor sections) were stained for SA-βGal detection using the Senescence β-galactosidase Staining Kit (#9860, Cell Signaling). Cells were fixed in 4% PFA at room temperature for 15 min, and staining was performed by following the manufacturer's instructions and incubating the samples overnight at 37ºC without CO_2. Tumor

18

sections were fixed in 4% PFA for 45-60 min at room temperature, washed with PBS and incubated for 5 hours with the staining solution at 37ºC with no CO_2.

Immunoblotting

Cells were washed with PBS and lysed with 150-200µL of lysis buffer (25mM Tris HCl pH 7.5, SDS 1%, 1mM EDTA pH 8 and protease inhibitors) supplemented with fosfatase inhibitor for pRb analysis. Cells were then harvested, passed through a 25G needle several times and boiled for 10min. Protein quantification was performed using the BCA method. Lysates were resolved in 6-12% acrylamide/bis-acrylamide gels, transferred to nitrocellulose membranes (#10600003, Acefesa) and immunoblotted following standard procedures.

Primary antibodies: Phospho-Rb (Ser807/811) (D20B12) antibody (#8516, #9308, Cell Signaling); AR antibody (#ab3590; Abcam); BCL-xL antibody (#2764, Cell Signaling); Bim antibody (#2819, Cell Signaling);

Secondary antibodies: anti-Rabbit IgG peroxidase antibody (#A6154, Sigma); peroxidase conjugate-goat anti-Mouse IgG antibody (#A4416, Sigma).

Ki67 immunofluorescence

Cells were fixed with 4% PFA, permeabilized with 0.3% triton X-100 and blocked with 5% BSA for 1h. Then cells were labelled with the primary antibody solution (1% BSA, 0.3% triton X-100) containing Ki-67 (D3B5) Rabbit (#9129, Cell Signaling), overnight at 4ºC. A following incubation with anti-rabbit IgG Fluor Goat 633 (#A21071, Fisher) was performed for 2h at room temperature. For image visualization coverslips were prepared in mounting medium and analysed in a Leica TCS-SP2-AOBS confocal microscope.

Colony formation assay

Control and senescent cells were seeded at different densities in 24-well plates and incubated in a CO_2 incubator at 37°C for 1 week. Colonies were fixed with 4% PFA and stained with 0.05% crystal violet solution.

BH3 profiling assay

Control and senescent cells were treated or non-treated with free navitoclax 0.3µM for 24 hours and mitochondrial activity was measured using the plate-based JC-1 BH3 profiling assay previously described by Letai *et al*.[66] Control and senescent cells were seeded in a 96-multiwell plate at a concentration of 200000 cells/well in DTEB buffer (135mM trehalose, 10mM HEPES-KOH pH 7.5, 50mM KCl, 0.1% BSA, 5mM succinate, 0.02mM EGTA, 0.02mM EDTA in distilled water and pH 7.5). Once plated, 100µL of supplemented DTEB (125µM oligomycin, 0.10mg/mL digitonin, 10µM JC1 and 50mM β-mercaptoethanol) and 2µL DMSO / 2µL BH3 peptides / 1µL FCCP were added to each well. Mitochondrial charge was measured by JC-1 red fluorescence over 3 hours in a PerkinElmer Multimode Plate Reader EnsightTM.

Cell viability assays

4T1 control and senescent cells (previously one week treated with Palbociclib 5µM) were seeded in flat-bottom clear white p96-multiwell plate at 3500 and 7500 cells/well concentration, respectively. Next day free navitoclax, **Gal·NP(Nav)** or **Gal·NP(0)** treatments were added at different concentrations (0.03-20µM for free formulation; 0.01-2mg/mL for **Gal·NP** previous filtration – 0.45µm) and cells were incubated for 72 hours. Cell viability was measured by luminescence using the CellTiter-Glo® Luminescent Cell Viability Assay (#G7571/2/3,

Promega) in a PerkinElmer Life Sciences Wallac Victor2TM spectrophotometer. For colony formation assays cells were seeded at 35000 (control) and 75000 (senescent) cells/well and treated with free navitoclax 0.3µM or the equivalent **Gal·NP(Nav)** concentration. After 72 hours colonies were fixed with 4% PFA and stained with 0.05% crystal violet solution.

Annexin V apoptosis assay

For the apoptosis evaluation assays 4T1 control and senescent cells were treated, or non-treated, with navitoclax 0.6µM. After 72 hours of incubation, cells were labelled with Alexa fluoresceinisothiocyanate-conjugated Annexin V (BD Bioscience) plus propidium iodide according to the manufacturer's recommendations. Samples were analysed in the cytometer CytoFLEX S Beckman Coulter.

Cell-based caspase activation assay

4T1 senescent cells were seeded in 6-well plate at a cellular density of 1.5×10^5 cells/mL. The next day cells were treated with navitoclax (1µM) and when indicated with 5µM of caspase 3 inhibitor z-VAD-FMK (ALX-260-020; Enzo Life Sciences). 48 hours later, cells were harvested and S100 cytosolic extracts were obtained. Total protein (50 µg) was mixed with assay buffer (PBS, 10% glycerol, 0.1mM EDTA, 2 mMDTT) containing 20µM Ac-DEVD-afc substrate. Activity was monitored using a Victor 2 spectrofluorimeter.

Confocal microscopy with Gal·NP(ICG)

Control and senescent cells were seeded on 6-multiwell plates at a concentration of 150000 cells/mL. Next day, a suspension of 1mg/mL **Gal·NP(ICG)** – previously filtered – was added

21

and cells and nanoparticles were incubated together for 6 hours and then washed with PBS in order to eliminate non-internalized nanoparticles. For confocal microscopy, coverslips were mounted and Hoechst and a plasmatic membrane dye (WGA Alexa Fluor 488 Conjugate, #W11261, ThermoFisher) were added for nuclei and membrane staining prior to cells visualization.

Animal model

Female BALB/cByJ wild type mice (28-34 days old) were purchased from Charles River Laboratories and maintained in ventilated racks under pathogen-free conditions at Principe Felipe Research Centre (Valencia, Spain), with food and water ad libitum and alternate dark and light cycles. All animals were treated humanely and experiments were approved by the Ethical Committee for Research and Animal Welfare.

Tumor formation

For each group 5 mice were used for statistical significance. Mice were anesthetized with isofluorane and the injection area was lightly shaved. Each animal was injected subcutaneously in the second lower right breast, with a cellular concentration of 0.5 million early passage 4T1 cells resuspended in 100µL of free-serum medium. Tumor growth was controlled every two days using an electronic caliper, and volume (mm^3) was estimated using the formula (length x width2)/2, were width was considered to be the shorter of two perpendicular diameters. Moreover, weight and animal welfare were also evaluated along all the treatments, attending to Morton and Griffiths scale criteria.

Mice treatments

Palbociclib for senescence induction was administrated by daily oral gavage (50-100 mg/kg) dissolved in sodium lactate 50mM at 16.5mg/mL.

For IVIS experiments to visualize nanoparticles localization, animals started palbociclib treatment one week post tumoral cell injection, and was daily maintained for one more week. Then **Gal·NP(ICG)** were intraperitoneally injected (200µL of a 10mg/mL suspension) and animals were observed in IVIS at different time points (6-24h post injection; ʎexc 745nm, ʎem 840 nm). Mice were finally euthanized in CO_2 atmosphere and organs were also observed *ex vivo* in IVIS.

For experiments with free or encapsulated navitoclax (#HY-10087, Medchemexpress), palbociclib administration began one day before starting the senolytic treatment and three days after 4T1 cells injection. Navitoclax was also daily administrated and maintained for 16 days, by oral gavage in case of free formulation (25 mg/kg, dissolved in 15%DMSO/PEG400) or by intraperitoneal injection (200µL of a 4 mg/mL suspension, equivalent to 2.5mg/kg of navitoclax) in case of **Gal·NP(Nav)**. At the end of the treatments animals were euthanized and organs were extracted for posterior evaluation.

For nanoparticles use, the corresponding nanoparticles were weighted in glass vials and resuspended in free-serum DMEM at the indicated concentrations, then were lightly sonicated in a water bath and stirred for 1 hour before administration. In vitro experimental calculations indicated that approximately 60mg of drug are deliverable per gram of nanoparticles.

Imaging by IVIS

For *in vivo* and *ex vivo* animals or organs fluorescence imaging after **Gal·NP(ICG)** treatments, an IVIS Spectrum Imaging System (Caliper LifeSciences) was used. For *in vivo* visualization, animals were anesthetized with 4-4.5% isofluorane in the induction period, and maintained with 2-2.5% during the scanning time. For *ex vivo* organs and tumors imaging, animals were euthanized at different time points after nanoparticles injection (6 or 24 hours) and organs were harvested and immediately analysed. Signal from **Gal·NP(ICG)** nanoparticles loaded with indocyanine green was detected using excitation and emission wavelengths of 745nm and 840nm, respectively. Fluorescence quantification was performed by Living Image® 4.3.1 software and was measured in photons per second per square centimetre per steradian $(p/s/cm^2/sr)$. Fluorophore release was quantified by manual drawing of regions of interest (ROIs) over the detected fluorescence signals in organs or tumors.

Metastases quantification

Lungs were collected after euthanasia and fixed in 4% PFA. Paraffin-embedded tissue sections on glass slides were processed for hematoxylin-eosin staining, and stained lung sections were scanned in a Leica Aperio Versa 200 equipment at 10x magnification. Metastatic 4T1 cell clusters were microscopically counted in different lung sections from five animals per group.

Ki67 Inmunohistochemistry

Indirect immunoperoxidase immunostaining was performed on 4% PFA-fixed paraffin-embedded tumor samples by an automated immunostaining platform (Leica Microsistems Bond RXm). Sections were incubated with the primary antibody Ki67 (D3B5) (#9129, Cell Signaling)

and then with the corresponding secondary antibody. Slides were counterstained with hematoxylin, dehydrated, and coverslipped.

Caspase 3 Immunofluorescence

Tumor sections (8µm) were fixed in 4% PFA and blocked with 5% goat serum, 0.1% Triton X-100 in PBS. Samples were labelled with caspase 3 active antibody (#9661; Cell Signaling) followed by anti-rabbit IgG conjugated to Alexa Fluor 488 (Life Technologies). Confocal images of ten different fields per sample were captured with a Leica SP8 microscope. Quantification of caspase 3 signal was performed evaluating the mean fluorescence value of the different fields using the ImageJ software analysis.

Silica biodistribution

Selected organs (lungs, liver, spleen, kidneys and tumor) were harvested and conserved for silicon (Si) detection. Organs were first weighted and then individually introduced in polytetrafluoroethylene (PTFE) bottles. 1mL of tetramethylammonium hydroxide solution (TMAH, #331635, Sigma) was added to each recipient, bottles were firmly closed and digestion was carried out for 2h at 80°C using a digestion unit Bloc digest 20 (Selecta). After cooling, digested samples were diluted with milliQ water to 10 mL in polypropylene Erlenmeyer flasks, then filtered in 0.45µm filters (#17463443, Scharlab) and kept in polystyrene tubes until determination. For the analysis, 0.5mL of sample was diluted to 10mL with a solution of 2% nitric acid and 1% hydrochloric acid. Silicon determination was performed in an Inductively Coupled Plasma Mass Spectrometer System (ICP-MS) Agilent 7900 in H_2 mode, using germanium as internal standard. A calibration curve was also prepared from silicon standard for

ICP (#08729, Sigma), and standard solutions were digested and treated exactly the same way as

the mice samples. Data are expressed as µg Si/g sample.

Statistical analysis

Statistical analysis of data used GraphPad Prism software. Comparisons of results between

groups were made by One-way ANOVA at 95% confidence or by Student's T-test.

Supporting Information
Supporting Information is available from the Wiley Online Library or from the author.

Author Contributions
The manuscript was written through contributions of all authors. All authors have given approval
to the final version of the manuscript.
R.M. and M.S: are co-founder and shareholder of Senolytic Therapeutics, Inc. (USA) and
Senolytic Therapeutics, S.L. (Spain).

Received: ((will be filled in by the editorial staff))
Revised: ((will be filled in by the editorial staff))
Published online: ((will be filled in by the editorial staff))

References

[1] A. Hernandez-Segura, J. Nehme, M. Demaria M. *Trends Cell Biol*. **2018**, 28, 436–53.

[2] L. Hayflick, P.S. Moorhead. *Exp Cell Res*. **1961**, 1.

[3] J.C. Acosta, J. Gil. *Trends Cell Biol*. **2012**, 22, 211–9.

[4] C.J. Sieben, I. Sturmlechner, B. Van de Sluis, J.M. Van Deursen. *Trends Cell Biol*. **2018**, 28, 723–37.

[5] J.W. Goldman, P. Shi, M. Reck, L. Paz-Ares, A. Koustenis, K.C. Hurt. *Clin Lung Cancer*. **2016**, 17, 80–4.

[6] R.S. Finn, J. Dering, D. Conklin, O. Kalous, D.J. Cohen, A.J. Desai, *et al*. *Breast Cancer Res*. **2009**, 11, 1–13.

[7] B. Geoerger, F. Bourdeaut, S.G. DuBois, M. Fischer, J.I. Geller, N.G. Gottardo, *et al*. *Clin Cancer Res*. **2017**, 23, 2433–41.

[8] D. Kwapisz. *Breast Cancer Res Treat*. **2017**, 166, 41–54.

[9] S. Pernas, S.M. Tolaney, E.P. Winer, S. Goel. *Ther Adv Med Oncol*. **2018**, 10, 1-15.

[10] R.L. Sutherland, E.A. Musgrove. *Breast Cancer Res*. **2009**, 11, 2–3.

[11] D.W. Fry, P.J. Harvey, P.R. Keller, W.L. Elliott, M. Meade, E. Trachet, *et al*. *Mol Cancer Ther*. **2004**, 3, 1427–38.

[12] J.A. Beaver, L. Amiri-Kordestani, R. Charlab, W. Chen, T. Palmby. A. Tilley, *et al*. *Clin Cancer Res*. **2015**, 21, 4760–6.

[13] R. Finn, J. Crown, I. Lang, K. Boer K. *Elsevier*. **2015**, 1.

[14] J.W. Chiu, G. Kwok, T. Yau, R. Leung R. *Transl Cancer Res*. **2017**, 6, S376–9.

[15] T. Traina, K. Cadoo, A. Gucalp. *Breast Cancer Targets Ther*. **2014**, 6, 123.

[16] N.C. Turner, J. Ro, F. André, S. Loi, S. Verma, H. Iwata, *et al*. *N Engl J Med*. **2015**, 373, 209–19.

[17] M. Cristofanilli, N.C. Turner, I. Bondarenko, J. Ro, S.A. Im, N. Masuda, *et al*. *Lancet Oncol*. **2016**, 17, 425–39.

[18] S. Lee, C.A. Schmitt. *Nat Cell Biol*. **2019**, 21, 94–101.

[19] S. Giaimo, F. D'Adda di Fagagna. *Aging Cell*. **2012**, 11, 378–83.

[20] D. Muñoz-Espín, M. Serrano. *Nat Rev Mol Cell Biol*. **2014**, 15, 482–96.

[21] F. Rodier, J. Campisi. *J Cell Biol*. **2011**, 192, 547–56.

[22] S. He, N.E. Sharpless. *Cell*. **2017**, 169, 1000-1011.

[23] D. McHugh, J. Gil. *J Cell Biol*. **2018**, 217, 1–13.

[24] M. Schosserer, J. Grillari, M. Breitenbach. *Front Oncol*. **2017**, 7.

[25] J.A. Ewald, J.A. Desotelle, G. Wilding, D.F. Jarrard D.F. *J Natl Cancer Inst*. **2010**, 102, 1536–46.

[26] M. Demaria, M.N.O. Leary, J. Chang, L. Shao, S. Liu, K. Koenig, *et al*. *Cancer Discov*. **2017**, 7, 165–76.

[27] R.R. Gordon, P.S. Nelson. *Drug Resist Updat*. **2012**, 15, 123–31.

[28] E. Wieland, J. Rodriguez-Vita, S.S. Liebler, C. Mogler, I. Moll, S.E. Herberich, *et al*. *Cancer Cell*. **2017**, 31, 355–67.

[29] M. Milanovic, D.N.Y. Fan, D. Belenki, J.H.M. Däbritz, Z. Zhao, Y. Yu, *et al*. *Nature*. **2017**, 553, 96–100.

[30] S. Parrinello. *J Cell Sci*. **2005**, 118, 485–96.

[31] J.L. Kirkland, T. Tchkonia, Y. Zhu, L.J. Niedernhofer, P.D. Robbins. *J Am Geriatr Soc*. **2017**, 65, 2297–301.

[32] B.G. Childs, M. Gluscevic, D.J. Baker, R.M. Laberge, D. Marquess, J. Dananberg, *et al*. *Nat Rev Drug Discov*. **2017**, 16, 718–35.

[33] B. Lozano-Torres, A. Estepa-Fernández, M. Rovira, M. Orzáez, M. Serrano, R. Martínez-Máñez, *et al*. *Nat Rev Chem*. **2019**.

[34] Y. Zhu, T. Tchkonia, H. Fuhrmann-Stroissnigg, H.M. Dai, Y.Y. Ling, M.B. Stout, *et al*. *Aging Cell*. **2016**, 15, 428–35.

[35] E. Wang. *Cancer Res*. **1995**, 5585, 2284–92.

[36] M.P. Baar, R.M.C. Brandt, D.A. Putavet, J.D.D. Klein, K.W.J. Derks, B.R.M. Bourgeois, *et al*. *Cell*. **2017**, 169, 132–147.

[37] Y. Zhu, T. Tchkonia, T. Pirtskhalava, A.C. Gower, H. Ding, N. Giorgadze, *et al*. *Aging Cell*. **2015**, 644–58.

[38] J. Chang, Y. Wang, L. Shao, R-M. Laberge, M. Demaria, J. Campisi, *et al*. *Nat Med*. **2015**, 22, 78–83.

[39] B.T. Kile. *Br J Haematol*. **2014**, 165, 217–26.

[40] E. Aznar, M. Oroval, L. Pascual, J.R. Murguía, R. Martínez-Mánez, F. Sancenón. *Chem Rev*. **2016**, 116, 561–718.

[41] A. Llopis-Lorente, B. Lozano-Torres, A. Bernardos, R. Martínez-Máñez, F. Sancenón. *J Mater Chem B*. **2017**, 5, 3069–83.

[42] F. Sancenón, L. Pascual, M. Oroval, E. Aznar. *ChemistryOpen.* **2015**, 418–37.

[43] M. Vallet-Regí, M. Colilla, I. Izquierdo-Barba, M. Manzano. *Molecules*. **2018**, 23, 1–19.

[44] Y.L. Su, S.H. Hu. *Pharmaceutics*. **2018**, 10, 1–21.

[45] C. Giménez, C. De La Torre, M. Gorbe, E. Aznar, F. Sancenón, J.R. Murguía, *et al*. *Langmuir*. **2015**, 31, 3753–62.

[46] A. Agostini, L. Mondragón, A. Bernardos, R. Martínez-Máñez, M. Dolores Marcos, F. Sancenón, *et al*. *Angew Chemie - Int Ed*. **2012**, 51, 10556–60.

[47] A. Bernardos, L. Mondragón, E. Aznar, M.D. Marcos, R. Martínez-Máñez, F. Sancenón, *et al*. *ACS Nano*. **2010**, 4, 6353–68.

[48] D. Muñoz-Espín, M. Rovira, I. Galiana, C. Giménez, B. Lozano-Torres, M. Paez-Ribes, *et al*. *EMBO Mol Med*. **2018**, e9355.

[49] P. Kau, G.M. Nagaraja, H. Zheng, D. Gizachew, M. Galukande, S. Krishnan, *et al*. *BMC Cancer*. **2012**, 12.

[50] W.D. Foulkes, I.E. Smith, J.S. Reis-Filho. *N Engl J Med*. **2010**, 363, 1938–48.

[51] K. Aysola, A. Desay, C. Welch, *et al*. *Hereditary Genet*. **2013**, Suppl 2.

[52] B.A. Pulaski, S. Ostrand-Rosenberg. *Curr Protoc Immunol*. **2001**.

[53] M. Collado, M. Serrano M. *Nat Rev Cancer*. **2010**, 10, 51–7.

[54] S. Goel, M.J. Decristo, A.C. Watt, H. Brinjones, J. Sceneay, B.B. Li, *et al*. *Nature*. **2017**, 548, 471–5.

[55] U.S. Asghar, A.R. Barr, R. Cutts, M. Beaney, I. Babina, D. Sampath, *et al*. *Clin Cancer Res*. **2017**, 23, 5561–72.

[56] G.P. Dimri, X. Leet, G. Basile, M. Acosta, G. Scorrt, C. Roskelley, *et al*. *Cell Biology*. **1995**, 92, 9363–7.

[57] B.Y. Lee, J.A. Han, J.S. Im, A. Morrone, K. Johung, E.C. Goodwin, *et al*. *Aging Cell*. **2006**, 5, 187–95.

[58] Y. Zhu, T. Tchkonia, T. Pirtskhalava, A.C. Gower, H. Ding, N. Giorgadze, *et al*. *Aging Cell*. **2015**.

[59] D.S. Potter, A. Letai. *Cold Spring Harb Symp Quant Biol*. **2016**, LXXXI:030841.

[60]   C. Billard. *Mol Cancer Ther*. **2013**, 12, 1691–700.

[61]   M. Reers, S.T. Smiley, C. Mottola-Hartshorn, *et al*. *Methods Enzymol*. **1995**, 260, 406-17.

[62]   M.M. Sugrue, Y. Wang, H.J. Rideout, R.M.E. Chalmers-Redman, W.G. Tatton. *Biochem Biophys Res Commun*. **1999**, 261, 123–30.

[63]   B.R. Stab, L. Martinez, A. Grismaldo, A. Lerma, M.L. Gutiérrez, L.A. Barrera, *et al*. *Front Aging Neurosci*. **2016**, 8, 1–10.

[64]   D. Wang, Y. Liu, R. Zhang, F. Zhang, W. Sui, L. Chen, *et al*. *Oncotarget*. **2016**, 7.

[65]   D.J. Baker, T. Wijshake, T. Tchkonia, N.K. LeBrasseur, B.G. Childs, B. Van de Sluis, *et al*. *Nature*. **2011**, 479, 232–6.

[66]   T.T. Vo, J. Ryan, R. Carrasco, D. Neuberg, D.J. Rossi, R.M. Stone, *et al*. *Cell*. **2012**, 151, 344–55.

Figures and legends
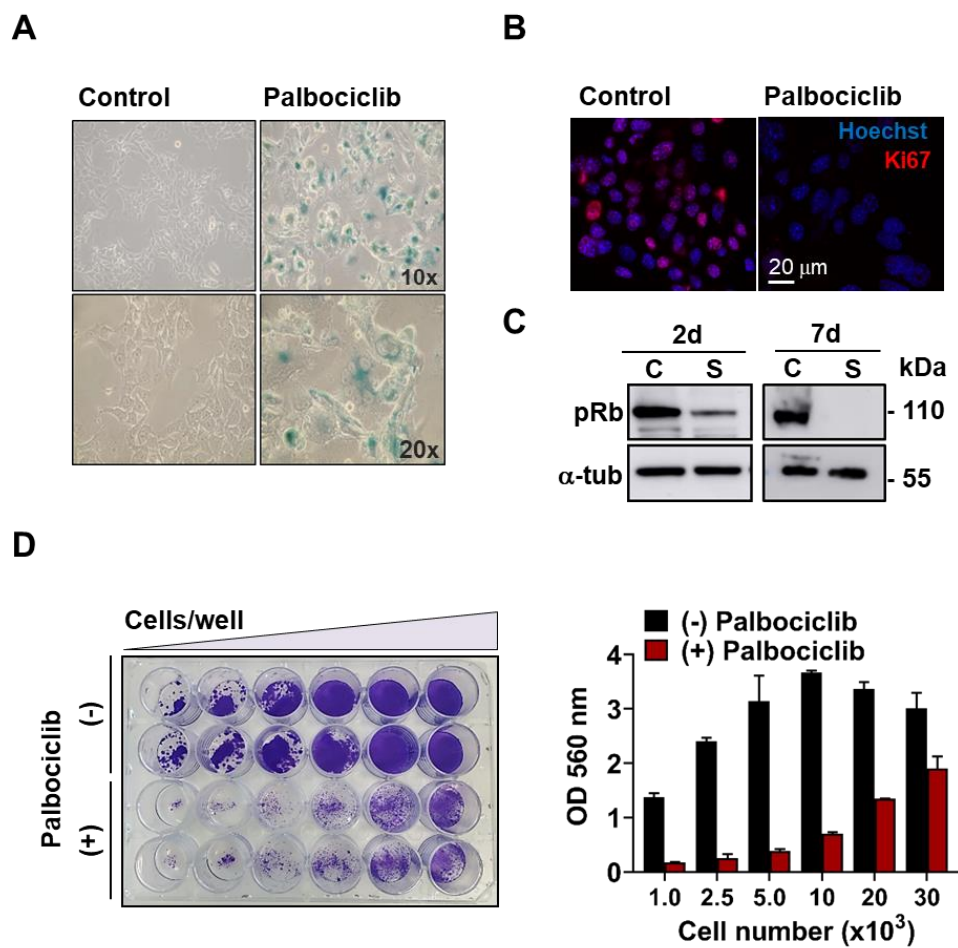
Figure 1. Palbociclib induces senescence in 4T1 triple negative breast cancer cells. A) β-galactosidase activity increases in 4T1 cells treated with palbociclib. 4T1 breast cancer cells were treated with palbociclib 5µM for one week, and senescence induction was confirmed by a β-galactosidase activity staining assay (blue signal) in both control and senescent cells. B) Decrease in the expression of the proliferation marker Ki67 upon senescence induction with palbociclib. Confocal microscopy images of immunofluorescence staining of Ki67 (red). Nuclei were stained with Hoechst (blue). C) pRb decreases upon palbociclib treatment. 4T1 cells were treated with palbociclib 5µM and total protein extracts were obtained at day 2 and day 7 to perform western blot analysis of the phosphorylated retinoblastoma protein (pRb) (expected band at 110kDa). Tubulin determination was included as loading control. D) 4T1 cells treated with palbociclib become cell cycle arrested. Cell proliferation studies of control and one week palbociclib-treated 4T1 cells. Increasing cell concentrations were seeded in different 24-plate wells (1000, 2500, 5000, 10000, 20000 and 30000; from left to right) and were let to proliferate for one week. Cell cycle arrest was confirmed by crystal violet staining. Graph represents quantification of violet colour by absorbance at 560nm.
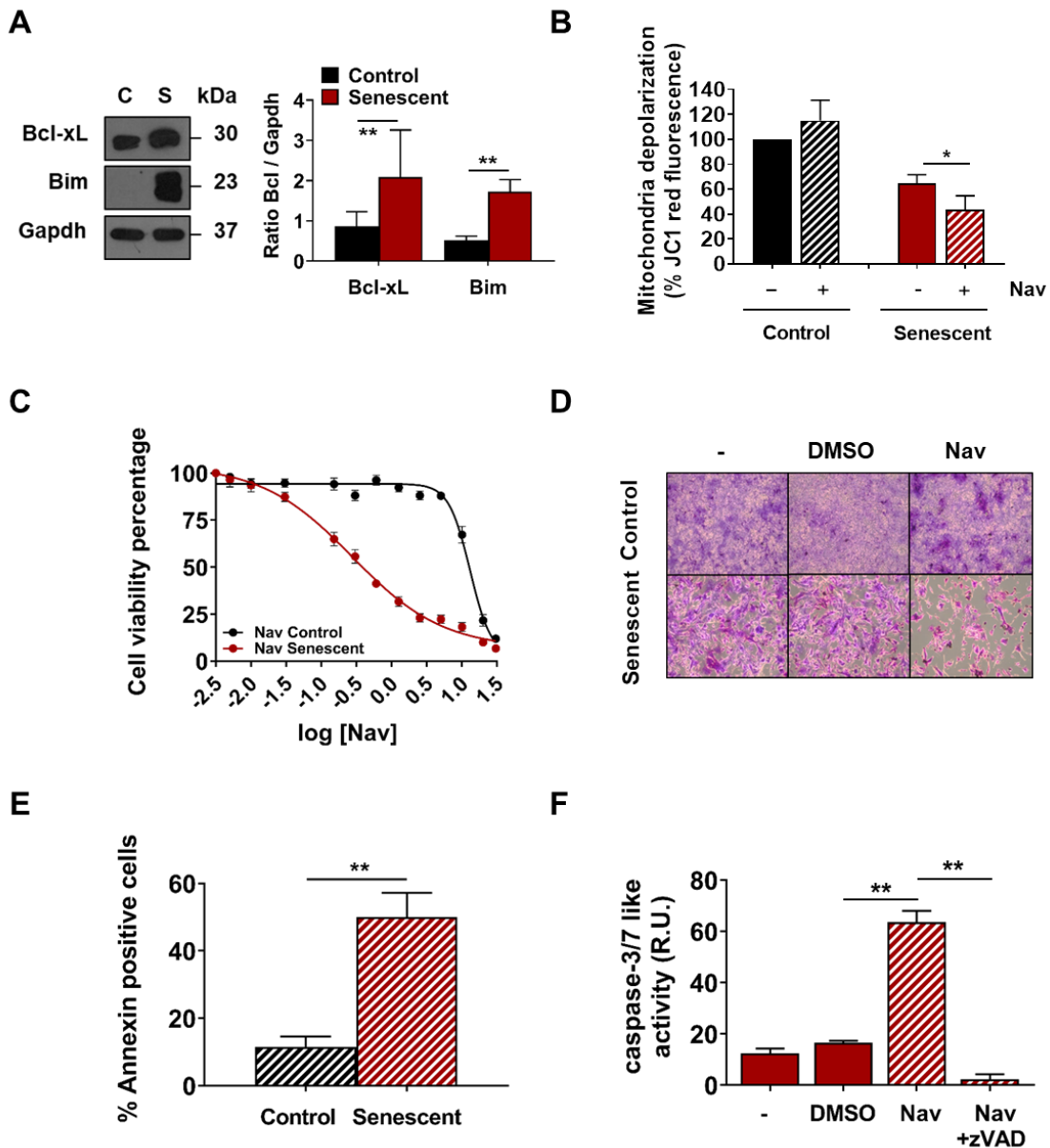
Figure 2. Navitoclax treatment induces senolysis in 4T1 palbociclib-treated cells. A) Anti-apoptotic Bcl-xL protein is over-expressed in palbociclib treated cells. Bcl-2 protein expression profile in control and senescent 4T1 cells analysed by western blot (left panel). Quantification of the bands using Gapdh as loading control (n=4) (right panel). Values are expressed as mean ± SD and statistical significance was assessed by the two-tailed Student's T-test: **$p < 0.05$. B) Navitoclax treatment produces depolarization of mitochondria from 4T1 senescent cells. Red fluorescence analysis of the JC-1 probe was used to measure mitochondria depolarization (n=3). Values are expressed as mean ± SEM and statistical significance was assessed by the two-tailed Student's T-test: *$p < 0.05$. C) Navitoclax induces cell death in 4T1 palbociclib-treated cells: control and senescent cells were treated with different concentrations of navitoclax (0.005 to 30μM) and cell viability was measured after 72 hours of treatment by luminescent ATP detection (n=6). D) Selective elimination of 4T1 senescent cells analysed by crystal violet staining. Cells

were treated with navitoclax at the IC50 concentration (0.3µM) for 72 hours. E) Treatment of 4T1 senescent cells with navitoclax induces the accumulation of annexin V positive cells. Flow cytometry analysis of annexin V staining in cells previously treated with navitoclax at the IC50 concentration (0.3µM) for 72 hours. Values are expressed as mean ± SEM and statistical significance was assessed by the two-tailed Student's T-test: **$p < 0.05$. F) Navitoclax treatment induces apoptosis in 4T1 senescent cells. Caspase 3/7 activity was measured upon described conditions. Values from three independent experiments are expressed as mean ± SD and statistical significance was assessed by the two-tailed Student's T-test: **$p < 0.05$.

A

Cargo (dye, drug) →

MSN

B

100 nm

50 nm

C

Release (%)

β-galactosidase

Blank

D

6 h · 24 h

Control

Senescent

Hoechst (nuclei), Alexa Fluor 488 (cell membrane), ICG (nanoparticles)

Confocal Ratio (ICG / Hoechst)

Control
Senescent

6h · 24h

**

*

E

Cell viability (%)

Nav Control
Nav Senescent
Gal·NP(Nav) Control
Gal·NP(Nav) Senescent

log [Nav]

F

DMSO · Nav · Gal·NP(Nav)

Control

Senescent

35
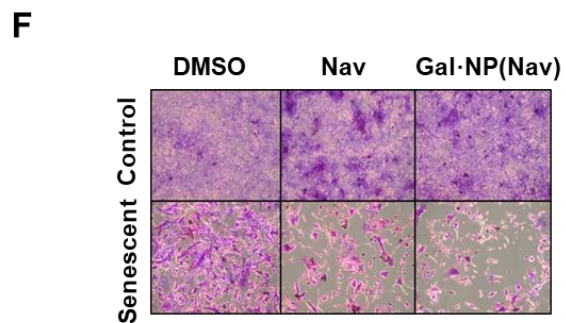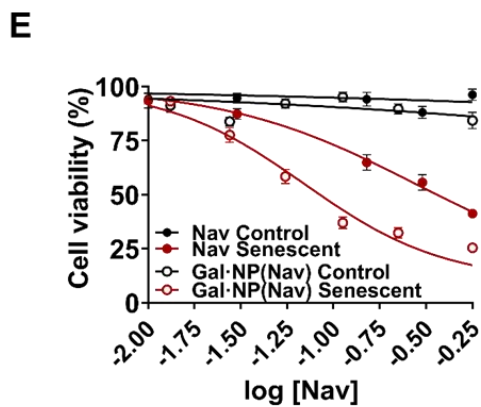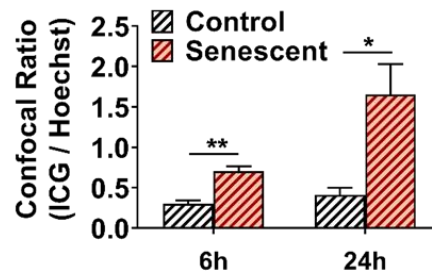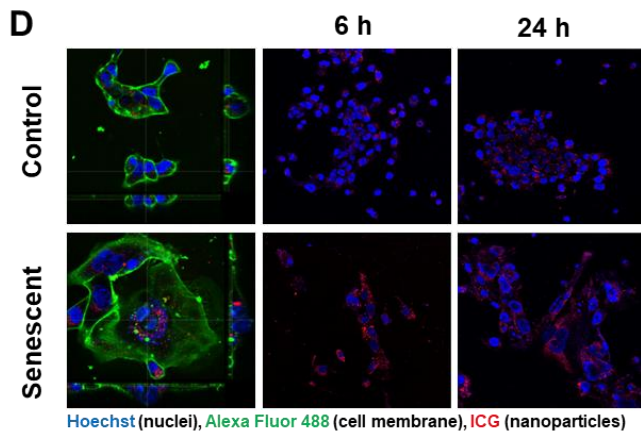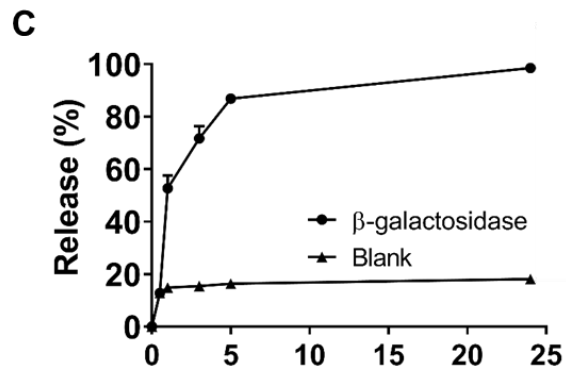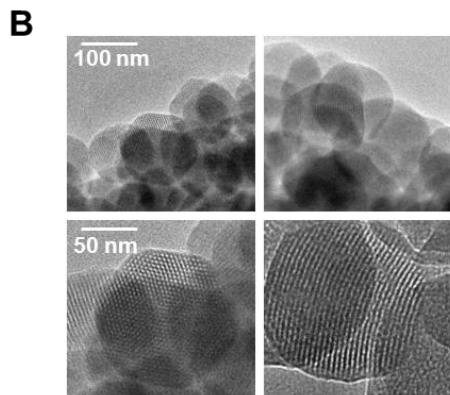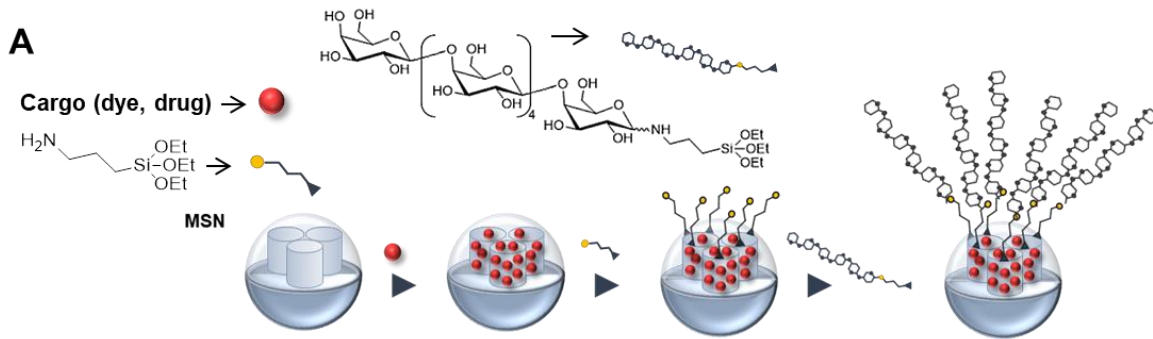
Figure 3. Gal·NP(Nav) selectively release the cargo in a β-galactosidase dependent manner.
A) Schematic representation of the gated nanoparticles and their synthesis. Mesoporous silica nanoparticles are loaded with the cargo (either ICG or navitoclax). Once loaded, the nanoparticles are functionalized in the external surface with (3-aminopropyl)triethoxysilane. Finally the hexa-galacto-oligosaccharide is covalently grafted onto the outer surface of the nanoparticles through the formation of a hemiaminal bond. B) Representative high resolution TEM images of Gal·NP. Spherical nanoparticles of ca. 100nm are observed, as well as the honeycomb structure of the porous scaffold or the channels as black and white longitudinal stripes. Scale bar: 50nm (down), 100nm (up). C) Cargo release studies of **Gal·NP(Nav)**, measured in absorption emission spectrometry. The graph shows the release profile of the load in the absence (blank) and in the presence of β-galactosidase from *Aspergillus oryzae* in water at pH 4.5 at room temperature at the indicated time points. D) **Gal·NP(ICG)** internalizes preferentially in senescent cells. Confocal analysis of control and senescent cells incubated with the fluorophore-loaded nanoparticles for 6 or 24 hours. Blue: Hoechst; Green: WGA Alexa Fluor 488 Conjugate; Red: ICG. Values are expressed as mean ± SEM and statistical significance was assessed by the two-tailed Student's T-test: $p < 0.05$. E-F) Treatment of 4T1 senescent cells with **Gal·NP(Nav)** induces cell death. Cell viability studies at different free or encapsulated navitoclax concentrations by i) luminescent ATP detection (left panel), or ii) crystal violet at the free navitoclax IC50 concentration (0.3µM, right panel).
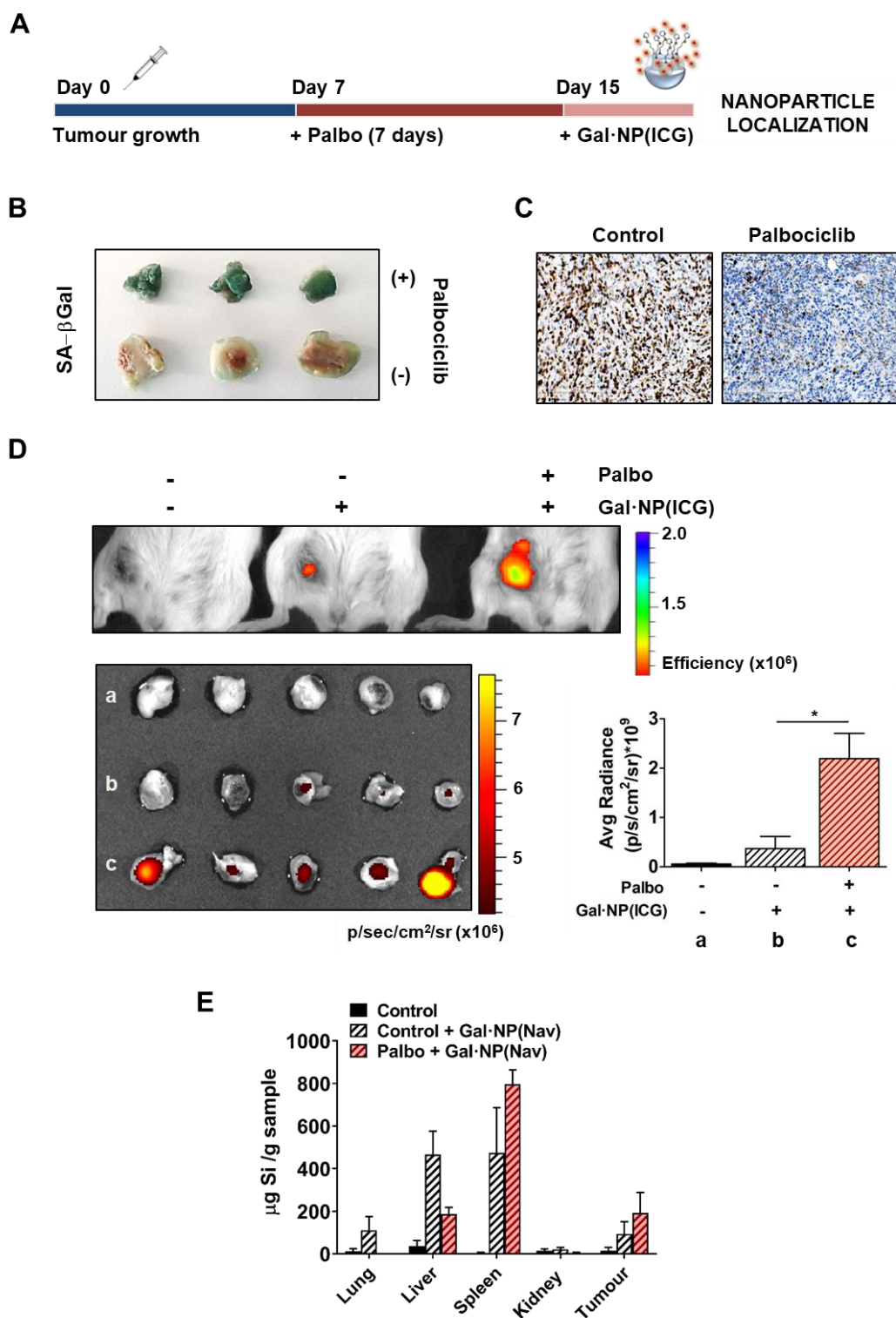
A

Day 0 — Tumour growth — Day 7 — + Palbo (7 days) — Day 15 — + Gal·NP(ICG) — NANOPARTICLE LOCALIZATION

B

SA−βGal

(+) / (−) Palbociclib

C

Control   Palbociclib

D

| - | - | + | Palbo |
| - | + | + | Gal·NP(ICG) |

2.0
1.5
Efficiency (x10⁶)

a
b
c

7
6
5

p/sec/cm²/sr (x10⁶)

Avg Radiance (p/s/cm²/sr)*10⁹

*

Palbo	-	-	+
Gal·NP(ICG)	-	+	+
	a	b	c

E

■ Control
▨ Control + Gal·NP(Nav)
▨ Palbo + Gal·NP(Nav)

μg Si /g sample

1000
800
600
400
200
0

Lung   Liver   Spleen   Kidney   Tumour

Figure 4. *In vivo* **senescence induction by palbociclib and targeting with Gal·NP(ICG).** A) Temporal scheme of palbociclib treatment in 4T1 orthotopic mice model to evaluate senescence induction. Tumors were grown for one week after cells injection, and then palbociclib treatment

was administered by oral gavage (50mg/kg) for 7 days. **Gal·NP(ICG)** were intraperitoneally injected (100mg **Gal·NP(ICG)**/kg) and animals were examined in IVIS at 6 and 24 hours post-administration to evaluate the nanoparticles localization. B) Palbociclib induces senescence in 4T1 TNBC. β-galactosidase staining of breast tumors (blue). C) The proliferation marker Ki67 decreases in palbociclib treated tumors. Ki67 detection by immunohistochemistry of tumor sections. D) **Gal·NP(ICG)** nanoparticles are able to selectively release the cargo in tumors of palbociclib-treated animals. *In vivo* and *ex vivo* analysis by IVIS spectrum imaging system. The upper panel shows the *in vivo* images from IVIS. The lower panel shows the *ex vivo* fluorescence signal in tumors and its corresponding emitted fluorescence quantification by Living Image® 4.3.1 software. Values (n=5) are expressed as mean ± SEM and statistical significance was assessed by the two-tailed Student's T-test: *p < 0.05. E) Biodistribution of the nanoparticles. Silicon is analysed by Inductively Coupled Plasma Mass Spectroscopy (ICP-MS). Data are expressed as mean ± SEM and represented as µg Si / g sample.
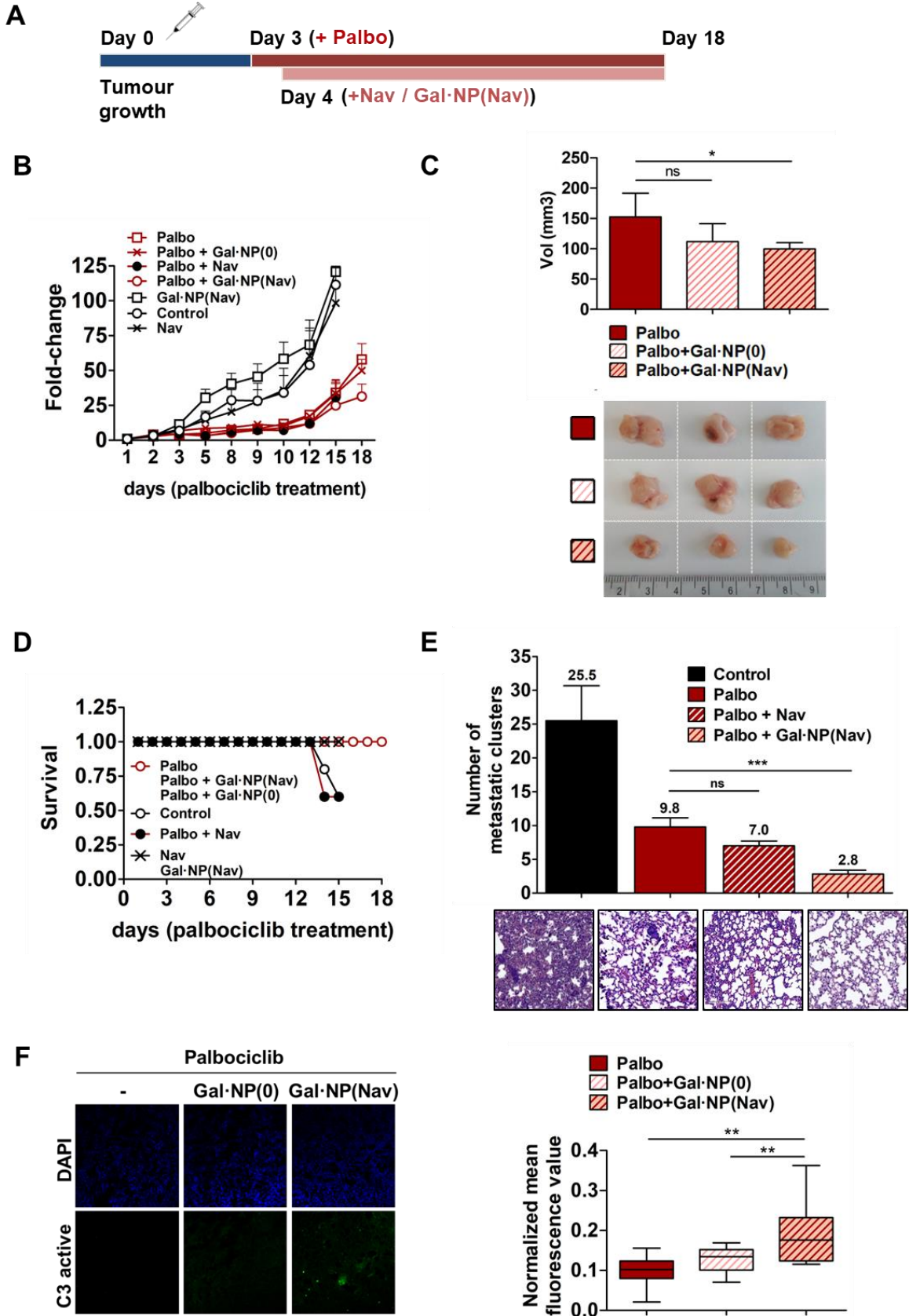
Figure 5. Senolysis by Gal·NP(Nav) reduces tumor size safely and effectively. A) Temporal scheme of palbociclib treatment in 4T1 orthotopic mice model followed by the senolytic treatment with free or encapsulated navitoclax. Three days after 4T1 cells injection, palbociclib treatment was started and daily maintained for 17 days (oral gavage, 100mg/kg). A day after palbociclib initiation, the senolytic treatment started and was daily maintained for 16 days (free navitoclax: oral gavage, 25mg/kg; **Gal·NP(Nav)**: intraperitoneal injection, 40mg **Gal·NP(Nav)**/kg (equivalent to 2.5mg/kg of free Navitoclax). B) Co-treatment with palbociclib plus **Gal·NP(Nav)** reduces tumor growth. Balb/cByJ female mice were orthotopically injected with 4T1 breast cancer cells and treated daily with vehicle or palbociclib and free navitoclax or **Gal·NP(Nav)** alone or in combination, at the indicated doses in A). For each tumor, the relative volume change was calculated in comparison to its baseline prior to treatment. Values (n=5) are expressed as mean ± SEM. C) Representative image of the tumors from section B), in which an ex vivo volume size comparison is observed between palbociclib treatment versus palbociclib combination with capped empty nanoparticles (**Gal·NP(0)**) or encapsulated navitoclax (**Gal·NP(Nav)**). Tumor volumes at final day 18 are expressed in mm3 as mean ± SD (n=5) and statistical significance was assessed by One-way ANOVA: *p < 0.05. D) Encapsulation of navitoclax enhances mice survival. Graph representation of animals' survival during the experimental period. E) Combined palbociclib plus **Gal·NP(Nav)** treatment reduces lung metastases in 4T1 TNBC model. Metastatic 4T1 cells clusters were microscopically counted in different lung hematoxylin-eosin stained sections and plotted in the graph (n=5). Values are represented as mean ± SEM and statistical significance was assessed by One-way ANOVA: ***p<0.05. F) Active caspase 3 is only determined in palbociclib plus **Gal·NP(Nav)** co-treated tumors. Representative images of the immunofluorescence of active caspase-3 (left panel) and mean fluorescence value quantification (right panel) in tumor sections. Statistical significance was assessed by One-way ANOVA: **p<0.05.

TOC

Keyword: nanotherapeutic senolysis
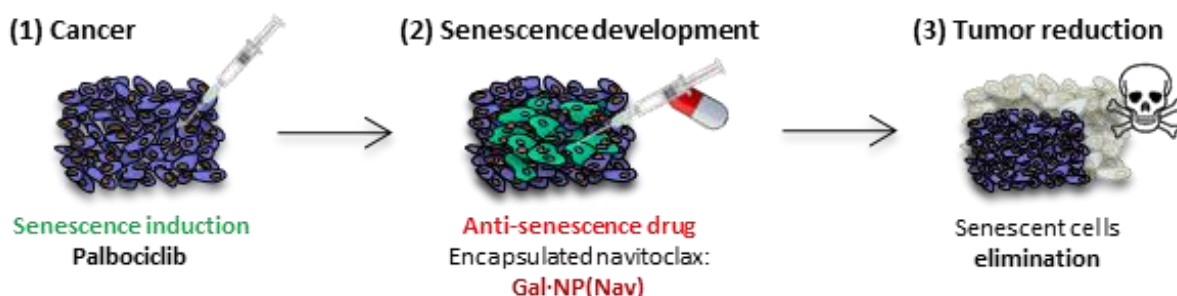
A combination of senogenesis (senoinduction with palbociclib) with nanoformulated targeted senolysis (encapsulated navitoclax) in triple negative breast cancer (TNBC) is described. Results show that treatment of TNBC with palbociclib and further elimination of senescent cells with encapsulated navitoclax in galacto-oligosaccharide capped nanoparticles (Gal·NP(Nav)) has benefit in tumor development, reduces metastases formation and diminishes navitoclax systemic toxicity.

Supporting information

Nanoparticles synthesis scheme
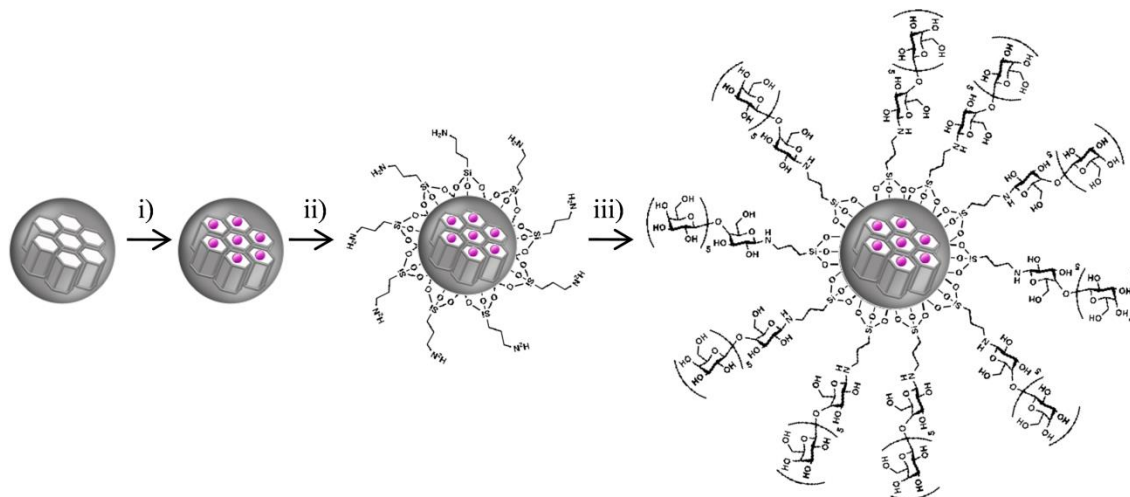
Figure S1. Schematic representation of the synthesis of loaded Gal·NPs. MCM-41 type scaffolds are loaded with ICG or navitoclax (i) and functionalized with APTES (ii). Finally, the beads are capped with β(1,4)-hexagalacto-saccharides (iii) to obtain the final Gal·NP.

Materials characterization

The PXRD of non-calcined nanoparticles (referred as "NPs as synthesized" in Muñoz-Espín et al (curve A in Figure S2), showed four low-angle reflections, typical of the hexagonal ordered array that can be indexed as (100), (110), (200) and (210) Bragg peaks. The removal of the surfactant and the condensation of silanol groups during the calcination step to obtain the starting mesoporous silica nanoparticles (starting NPs) are reflected in a slight shift of these peaks 2θ values (curve B in Figure S2). For **Gal·NP(0)** and **Gal·NP(ICG)** materials (curves C and D in Figure S2), the reflections (110) and (200) are lost, most likely due to a reduction of contrast. Nevertheless, the presence of the d100 peak in the XRD patterns indicated that the process of

pore loading and the additional functionalization with the corresponding saccharides did not to a

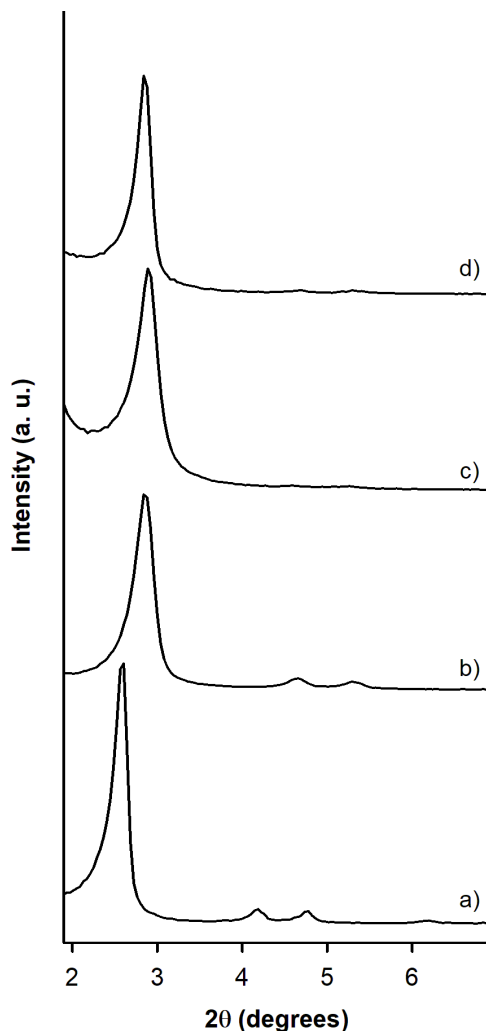large extent modify the mesoporous scaffolding.

Figure S2. Powder X-Ray diffraction patterns at low (left) and high (right) angles of: (a) NPs as synthesized, (b) starting NPs, (c) **Gal·NP(0)**, (d) the final solid containing indocyanine green **Gal·NP(ICG)**.

TEM analysis showed the presence of the mesoporous structure in the final functionalized solids

(Figure 3B, Figure S3). Figure S3 showed that the prepared NPs-based materials exhibit a

spherical geometry with diameter ca. 100 nm. Moreover, the typical channels of these MSNs matrix were visualized as alternate black and white stripes.
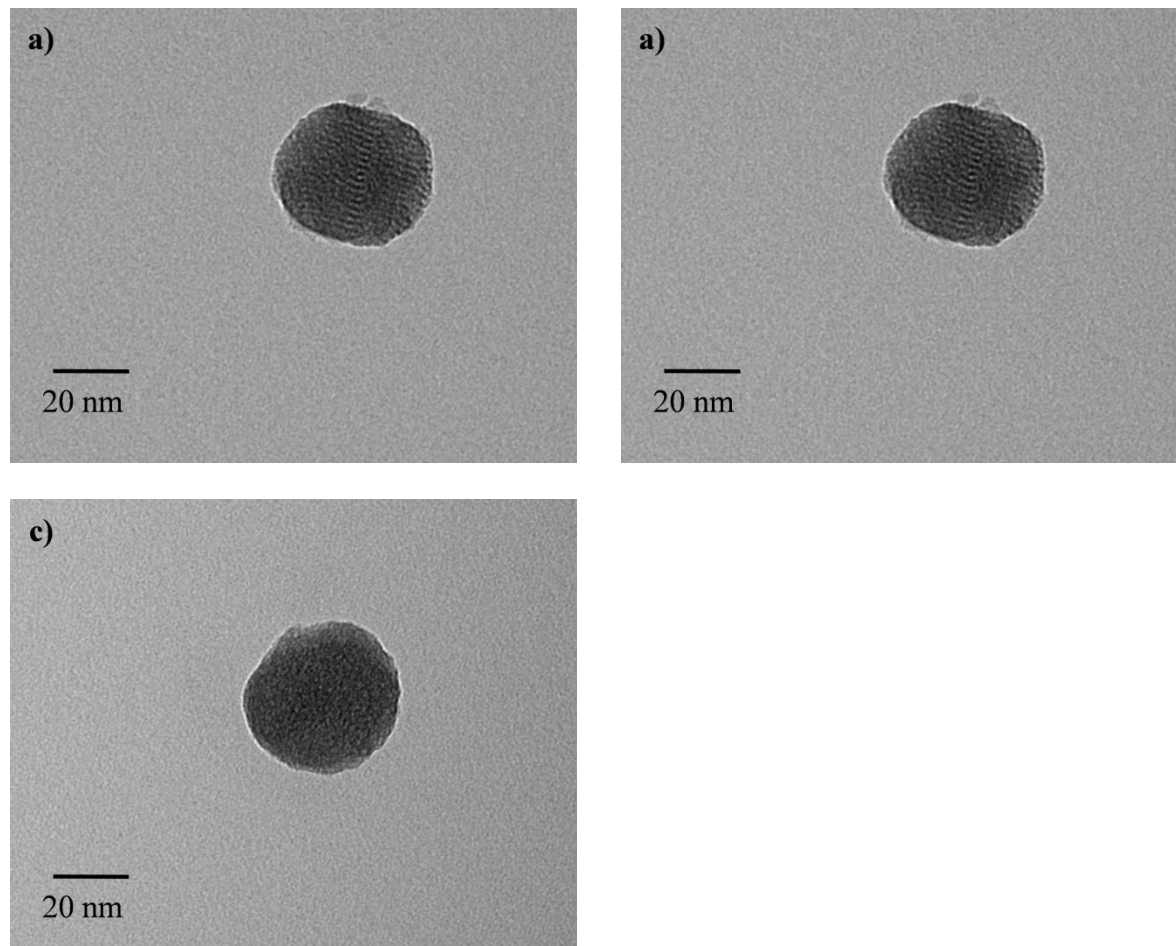

Figure S3. TEM analysis of: (a) starting NPs, (b) **Gal·NP(0)** and (c) **Gal·NP(ICG)**.

The N_2 adsorption-desorption isotherms of the calcined starting NPs showed two sharp adsorption steps (Figure S4A). The first step, at an intermediate P/P_0 value (0.1-0.3), is S-6 typical of this type of materials and attributed to nitrogen condensation inside the mesopores by capillarity. The absence of a hysteresis loop in this range and the tight BJH pore distribution (inset, Figure S4A), suggested the presence of uniform cylindrical mesopores with pore volume of 0.97 cm^3 g^{-1} calculated by using the BJH model on the adsorption branch of the isotherm.

44

Moreover, the total specific surface was calculated to be 1091.12 m^2 g^{-1} by the application of the BET model. On the other hand, N$_2$ adsorption-desorption isotherms of **Gal·NP(ICG)** and **Gal·NP(0)** showed a significant decrease in the adsorbed N$_2$ volume and surface area as a consequence of the functionalization inside the pores (Figure S4B and S4C). Parameters calculated from N$_2$ adsorption-desorption isotherms are listed in Table S1.
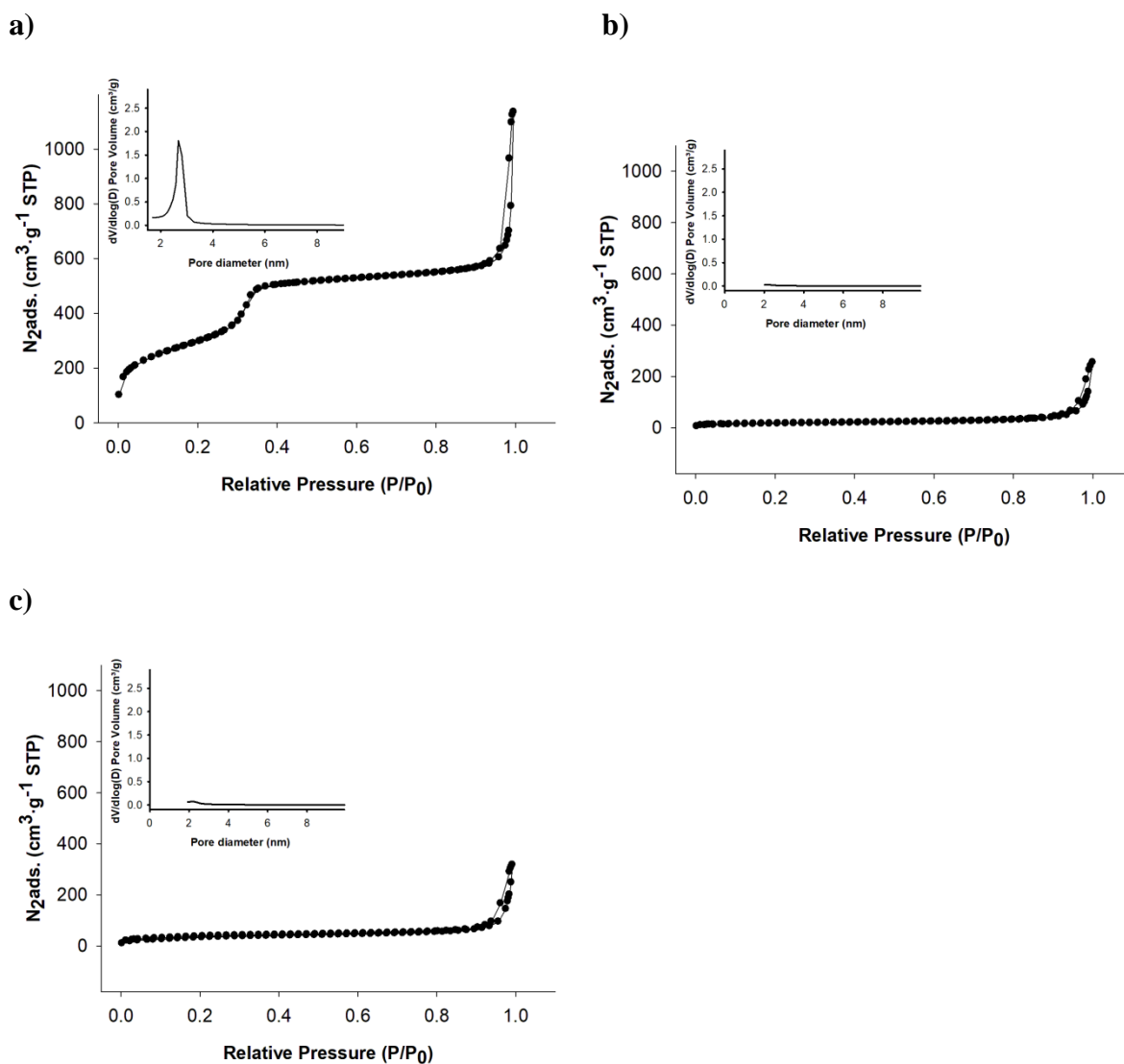
a)

b)

c)

Figure S4. N$_2$ adsorption-desorption isotherms for (a) starting NPs, (b) **Gal·NP(ICG)** and (c) **Gal·NP(0)**.

Table S1. BET specific surface values, pore volumes and pore sizes calculated from N_2 adsorption-desorption isotherms for selected materials.

Sample	S_{BET} $[m^2g^{-1}]$	Pore Volume $[cm^3g^{-1}]$	Pore size [nm]
Starting NPs	1091	0.97	2.79
Gal·NP(ICG)	57	0.05	--
Gal·NP(0)	126	0.1	--

From dynamic light scattering (DLS) measurements (Figure S5, Table S2), the hydrodynamic diameter of the starting MSNs and the final nanoparticles was determined, obtaining a single population distribution which indicated the good dispersion of the particles. The increase in the hydrodynamic diameter between starting NPs and Gal·NP was consistent with the external functionalization of the nanoparticles with the galacto-oligosaccharide.
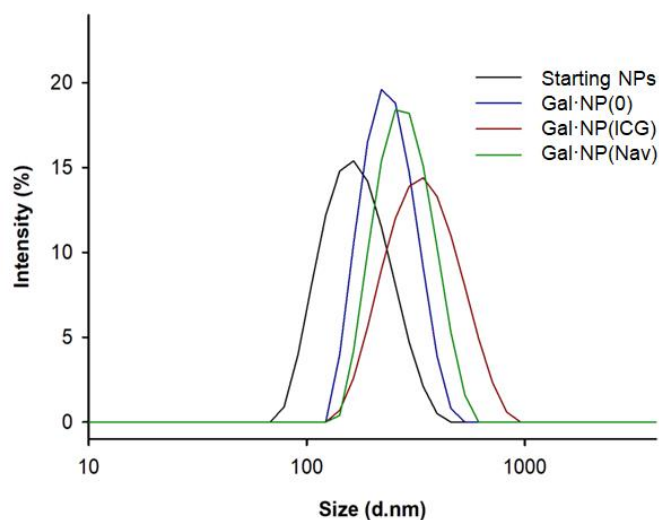
Figure S5. Dynamic Light Scattering (DLS) analysis that shows the hydrodynamic diameter of starting NPs (black line), **Gal·NP(0)** (blue line), **Gal·NP(ICG)** (red line) and **Gal·NP(Nav)** (red line).

Table S2. Hydrodynamic diameter and zeta potential of selected materials.

Solid	Hydrodynamic particle diameter (nm)	Zeta potential (mV)
Starting NPs	183 ± 8	- 31.2
Gal·NP(0)	249 ± 6	- 5.6
Gal·NP(ICG)	376 ± 18	- 13.5
Gal·NP(Nav)	301 ± 10	- 0.19

Cargo release studies of Gal·NP(ICG)

4 mg of **Gal·NP(ICG)** were suspended in 10mL of water at pH 4.5, stirred and this volume was separated into two suspensions of 5mL. Then, aliquots of 300µL were taken and 2µL of NaOH (0.15M) were added to each one. The mixtures were vigorously stirred for 3min and they were centrifuged for removing the solid. The aliquots were measured by emission spectroscopy to obtain the initial point. Then, 5mg of β-galactosidase from *Aspergillus oryzae* were added to one of the aliquots, and, after certain time 300µL of each suspension were taken, 2µL of NaOH (0.15M) were added, centrifuged and cargo released was measured (Figure S6).
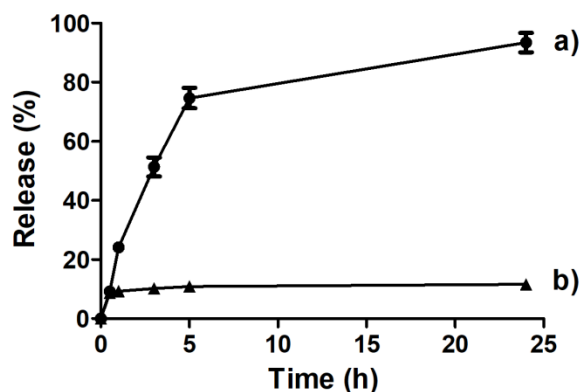

Figure S6. β-galactosidase dependent cargo release from **Gal·NP(ICG)**. Nanoparticles were suspended in absence (a) or presence (b) of β-galactosidase (4mg **Gal·NP(ICG)** /10mL water), aliquots were taken at different time points, centrifugated to eliminate the nanoparticles and fluorescence in the solution measured to quantify cargo released (ICG λem 840 nm).

Gal·NP(ICG) validation in 4T1 cells by flow cytometry

Control and senescent cells were seeded on 6-multiwell plates at a concentration of 150000 cells/mL. Next day, a suspension of 1mg/mL **Gal·NP(ICG)** – previously filtered – was added and cells and nanoparticles were incubated together for 6 hours and then washed with PBS in order to eliminate non-internalized nanoparticles. For flow cytometry assays, cells were detached

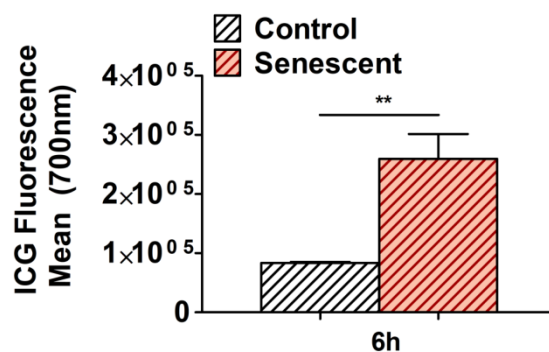and stained with Hoechst dye. Samples were analysed in the cytometer CytoFLEX S Beckman

Coulter.

Figure S7. Gal·NP(ICG) released their content more efficiently in palbociclib-senescent cells compared to control cells after 6 hours, in concordance with their high levels of β-galactosidase activity.

Cell toxicity studies with Gal·NP(0)

In order to first check the biocompatibility of the synthesized materials (and to be sure that the

expected cell death after the drug-loaded nanoparticles treatment would be because of the

navitoclax and no because of the mesoporous container), a 72 hours viability assay was

performed by treating 4T1 control and senescent cells with capped nanoparticles with no cargo,

Gal·NP(0). Results showed that the empty Gal-functionalized solid was harmless for the cells at

several studied concentrations, being the cell viability almost one hundred per cent in all cases
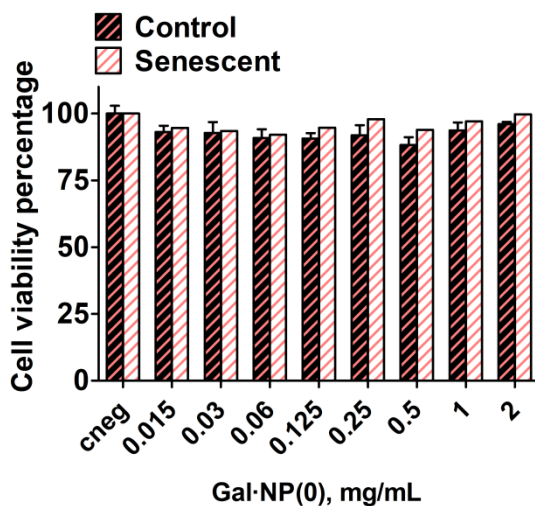
(Figure S8).

Figure S8. Cell viability assay with non-loaded nanoparticles **Gal·NP(0)** at different filtered concentrations was performed. Control and one week palbociclib treated 4T1 cells were exposed for 72 hours to no cargo nanoparticles to see the biocompatibility of the nanodevice. Experiments were repeated three times and media ± SEM is represented.
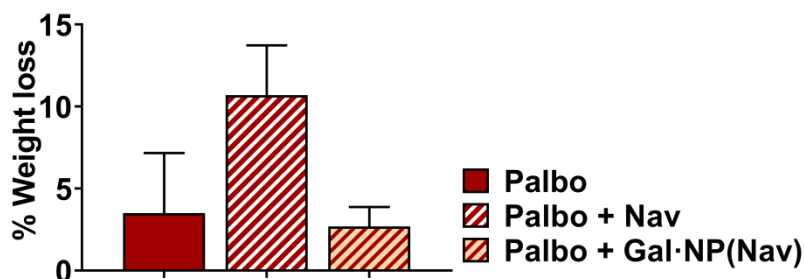
Weight loss in treated mice

Figure S9. Weight loss decreases in **Gal·NP(Nav)** treated animals. Weight loss percentages expressed as mean ± SEM.

Androgen receptor expression in 4T1 cells

The 4T1 murine breast cancer cell line was characterized in order to confirm its triple negative profile (data not shown). No signal was neither detected for the androgen receptor, which confirmed (according to Turner *et al*) that we were working with a 4T1 population candidate to be sensitive to palbociclib treatment (Figure S10).
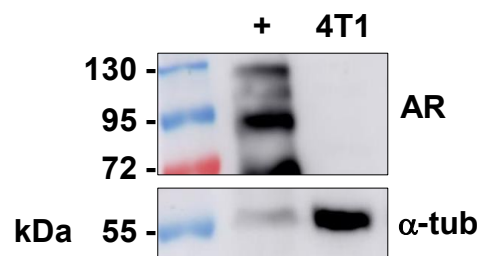
Figure S10. Western blot analysis was performed to characterize the molecular profile of the 4T1 murine breast cancer cells. VCaP cell line was used as positive control for AR marker (expected band at 110 kDa). Tubulin was determined as loading control.